Frontiers of Mid-IR Lasers Based on Transition Metal Doped Chalcogenides

Sergey B. Mirov, *Member, IEEE*, Igor S. Moskalev, Sergey Vasilyev, Viktor Smolski, Vladimir V. Fedorov, Dmitry Martyshkin, Jeremy Peppers, Mike Mirov, Alex Dergachev, and Valentin Gapontsev

(Invited Paper)

***Abstract*—Enabling broad tunability, high peak and average power, ultrashort pulse duration, and all known modes of laser operation—transition-metal (TM)-doped II–VI chalcogenides are the materials of choice for direct lasing in the mid-IR. The host materials feature broad infrared transparency, high thermal conductivity, low phonon cutoff, low optical losses, and are available as either single crystals or polycrystalline ceramics. Doped with TM ions, these media exhibit a four-level energy structure, the absence of excited state absorption, as well as broad absorption and emission bands. Doped single-crystals of high optical quality are difficult to grow; however, the advent of postgrowth diffusion doped ceramics has resulted in significant progress in laser development. Here, we summarize recent experimental laser results on Cr and Fe doped II–VI chalcogenides providing access to the 1.8–6 μm spectral range with a high (>60%) efficiency, multi-Watt-level [140 W in continuous wave (CW)] output powers, tunability of >1000 nm, short-pulse (<16 fs) multi-Watt oscillation, and multi-Joule output energies in free running and gain-switched regimes. We also review recent results on hybrid fiber-bulk (Er-fiber/Er:YAG, Tm-fiber: Ho:YAG/YLF) systems combining high efficiency of CW fiber lasers with high pulse energies of bulk materials and serving as pump sources of gain-switched Cr:II-VI lasers.**

***Index Terms*—Laser, laser tuning, laser mode locking, mid-infrared, solid-state lasers, transition metal, wide-band II-VI semiconductors, Cr:ZnSe, Cr:ZnS, Fe:ZnSe, hybrid fiber-bulk lasers, Ho:YAG, Ho:YLF, Er:YAG.**

Manuscript received December 18, 2017; revised February 8, 2018; accepted February 9, 2018. Date of publication February 20, 2018; date of current version July 27, 2018. This work was supported by IPG Photonics Corporation and in part by the Air Force Office of Scientific Research under Grant FA9550-13-1-0234, in part by Defense Advanced Research Projects Agency under Grant W31P4Q-15-1-0008, and in part by the Department of Energy under Grant DE-SC0018378. *(Corresponding author: Sergey B. Mirov.)*

S. B. Mirov, V. V. Fedorov, and D. Martyshkin are with the Center for Optical Sensors and Spectroscopies, Department of Physics, University of Alabama at Birmingham, Birmingham AL 35294 USA (e-mail: mirov@uab.edu; vfedorov@uab.edu; dmartych@uab.edu).

I. S. Moskalev, S. Vasilyev, M. Mirov, V. Smolski, and J. Peppers are with IPG Photonics, Southeast Technology Center, Birmingham, AL 35211 USA (e-mail: imoskalev@ipgphotonics.com; svasilyev@ipgphotonics.com; mmirov@ipgphotonics.com; vsmolski@ipgphotonicsc.com; jpeppers@ipgphotonics.com).

A. Dergachev and V. Gapontsev are with IPG Photonics Corporation, Oxford, MA 01540 USA (e-mail: adergachev@ipgphotonics.com; vgapontsev@ipgphotonics.com).

Color versions of one or more of the figures in this paper are available online at http://ieeexplore.ieee.org.

Digital Object Identifier 10.1109/JSTQE.2018.2808284

I. Introduction and Spectroscopic Properties

TM ION doped II-VI semiconductors have been extensively studied since the 1960 s by many research groups (see, for example [1]– [8]). However, the lasing of a Cr:ZnSe crystal was first reported in 1996 by scientists from Lawrence Livermore National Laboratory [9]. In this publication, the authors formulated the major features that make these materials so attractive for middle infrared (MIR) laser applications:

- Tetrahedral coordination of the TM ions in II-VI semiconductors gives approximately two times smaller crystal field energy splitting in comparison with typical octahedral coordination sites, placing the TM dopant transitions further into the infrared (IR).
- The crystal's heavy anions enable a very low energy optical phonon cut-off. This makes II-VI crystals transparent in a wide spectral range and decreases the rate of non-radiative relaxation, giving promise of a high yield of fluorescence at room temperature (RT).
- Strong electron-phonon coupling of the TM ions results in significant broadening (up to 50% of central wavelength) of their amplification band making TM:II-VI gain media of great interest for ultra-broad MIR tunability as well as for ultra-short pulse generation.
- Among a large group of TM ions Cr^{2+} $(3d^4)$ and Fe^{2+} $(3d^6)$ ions are the most attractive for laser applications. These chemically stable divalent dopant ions provide the 'right' multiplet structure for broadly tunable MIR lasers, including broad absorption and emission bands, high cross-sections, and the absence of excited state absorption.

The same group also demonstrated that, while II-VI chalcogenides are available in single crystal and in polycrystalline forms, their physical, spectroscopic, and laser characteristics are practically identical [10]. This was of particular importance since II-VI single-crystals of high optical quality are difficult to grow while chemically vapor grown II-VI polycrystals benefited from low-cost mass production technology of fabrication and were widely used as passive materials for middle-infrared technology [11]. The combination of low-cost and readily available polycrystalline II-VI materials with a quantitative and affordable post-growth TM doping procedure, preserving high optical quality of the starting materials, enabled an effective technology for fabrication of gain elements, which is

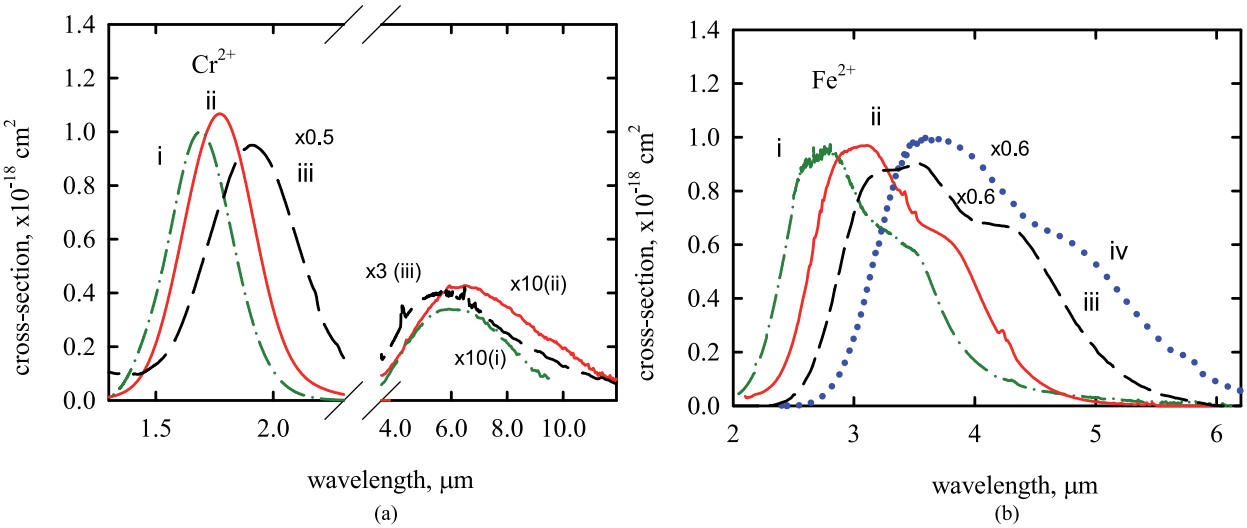

Fig. 1. Absorption cross section of Cr^{2+} (A) and Fe^{2+} (B) ions in ZnS (i), ZnSe (ii), CdSe (iii) and CdTe (iv) crystals at RT.

quite rare for solid-state laser materials [12]–[17]. Major material and spectroscopic characteristics, methods of fabrication, as well as information on lasing aspects of Cr and Fe doped II-VI chalcogenide are summarized in the following reviews [18]–[29]. In this review we will focus on the current progress in the development of solid state MIR lasers based on Cr^{2+} and Fe^{2+} doped polycrystalline ZnS and ZnSe hosts, since these gain media enable the most advanced output laser characteristics. Some other chalcogenide hosts will also be briefly discussed. We did not cover the use of TM:II-VI materials as passive Q-switches or mode-lockers since this topic deserves a separate review. Some information on this topic is available in [30].

A. *Overview of Spectroscopic Properties*

The ground state of the Cr^{2+} ($3d^4$) and Fe^{2+}($3d^6$) ions is the ^5D state. A ^5D ground state is split into $^5T_2$ triplet and ^5E duplet in the tetrahedral crystal field of II-VI chalcogenides. The transitions between these levels are in the MIR spectral region. All the transitions to other chromium and iron multiplets (^3H, ^3G, $^3F(2)$, ^3D, $3P(2)$, ^1I, $1G(2)$, ^1F, $^1D(2)$, $^1S(2)$) are spin forbidden. In the tetrahedral crystal field, doublet ^5E is the ground state of the iron ions, while $^5T_2$ is the ground state of the chromium ions. The low temperature structure of the emission and absorption bands could be explained by combinations of spin-orbit and dynamic/static Jan-Teller interactions as well as electron-phonon coupling [5]. Since there is no strong hierarchy over these interactions, the detailed energy structures are still subjects for theoretical interpretation. Below we will summarize some spectroscopic results of great importance for lasing.

1) Spectral Position of the Bands: Absorption and emission cross-sections of Cr and Fe ions in different II-VI hosts are depicted in Figs. 1 and 2, respectively. According to crystal field theory, energy splitting between $^5T_2$ and ^5E levels is proportional to d^{-5} (where d is the distance between ligands and transition metals). This explains why the shortest and the longest spectral positions of the absorption/emission bands are displayed in ZnS ($d = 2.34$ Å) and CdTe ($d = 2.81$ Å) crystals, respectively.

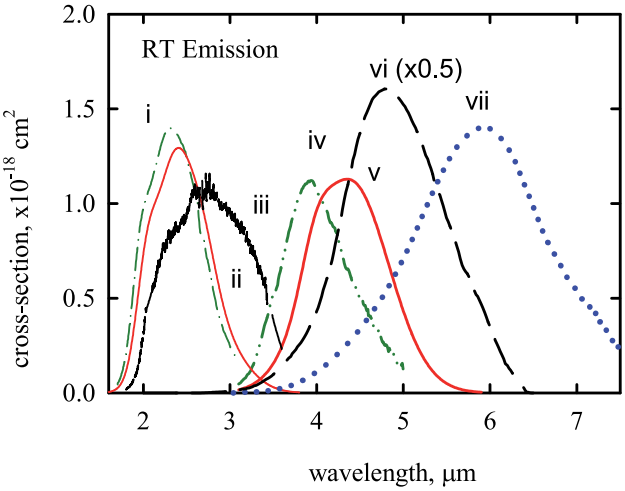

Fig. 2. Emission cross sections of Cr^{2+} ions in ZnS (i), ZnSe (ii), CdSe (iii) crystals and Fe^{2+} ions in ZnS (iv), ZnSe (v), CdSe (vi) and CdTe (vii) crystals at RT.

The energy splitting of the Fe^{2+}($3d^6$) ions are smaller than Cr^{2+} ($3d^4$) in the same hosts [9]. There is an additional MIR absorption band in the 4–8 μm spectral region in chromium doped II-VI crystals. This band results from additional splitting of the $^5T_2$ ground state. The absorption cross-section of this band is ~20 times smaller than that of 1.6–2.0 μm band.

2) Luminescence Quantum Yield (QY) and Radiative Lifetime: The radiative lifetimes of the Fe^{2+} ions in low concentration doped ZnS/ZnSe hosts are 55–57 μs (see Fig. 3) and are approximately ten times longer than those of Cr^{2+} ions ($\tau_{\rm rad} = 5-7\ \mu$s).

The RT luminescence QY of Cr^{2+} is approximately 100% for Cr:ZnSe (80% for Cr:ZnS), while luminescence of Fe^{2+} ions is strongly thermally quenched with the upper level lifetime at RT of only 50–380 ns. The QY of Fe:ZnSe at the low temperature limit is 100% while for Fe:ZnS it was measured to be only 10% [8].

Concentration quenching of Cr:ZnSe crystals at RT was revealed for chromium concentration in excess of 10^{19} cm^{-3} [14].

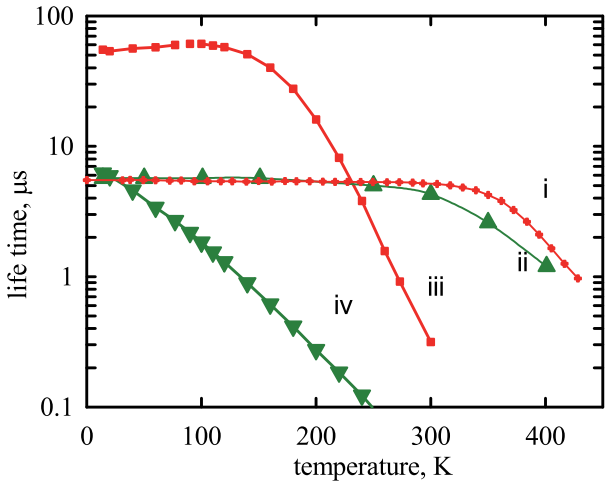

Fig. 3. Temperature dependences of MIR luminescence lifetimes in Cr:ZnSe (i), Cr:ZnS (ii); Fe:ZnSe (iii), and Fe:ZnS (iv) crystals.

In contrast, at RT thermal quenching is the dominant process in Fe:ZnSe. Shortening of the luminescence lifetime from 382 to 186 ns at RT was measured in a crystal with iron concentration of 1.1×10^{20} cm^{-3} [31]. The luminescence lifetime of Fe:ZnSe crystals with iron concentration of $\sim 10^{19}$ cm^{-3} featured an unexpected increase from 33 to 105 μs with a temperature increase from 12 to 120 K [32]. Similar measurements performed by our group [31] showed that with the use of samples with low iron concentration ($\sim 10^{17}$ cm^{-3}) the luminescence lifetime was constant ($\tau = 57$ μs) over 14–110 K temperature range. We believe that the unusual dependence of luminescence lifetime measured in [32] could be explained by energy migration and reabsorption of luminescence in highly doped Fe:ZnSe samples.

3) Inhomogeneous Broadening and Multi TM Center Formation: It is noteworthy that the concentration of the Cr(Fe) ions in ZnS(ZnSe) crystals in valence state other than 2+ is negligible [2]. Even in polycrystalline ZnSe samples doped by post-growth thermal diffusion method to the level of $\sim 10^{19}$ cm^3, the ratio of n_{Cr+}/n_{Cr2+} (n_{Fe3+}/n_{Fe2+}) was smaller than 10^{-5} [33].

There are no spectroscopic or electron spin resonance (EPR) experiments where formation of TM-TM pair complexes in ZnSe/ZnS crystals was clearly identified. However, the authors of [2] measured different positions of low temperature absorption spectra Zero-Phonon Lines (ZPL) in cubic and hexagonal ZnS crystals. The difference between ZPLs in these crystals was measured to be ~ 100 cm^{-1}, which indicates the sensitivity of the spectral position of ZPL to crystal field perturbation in the second coordination sphere. Two extra absorption ZPLs were measured at low temperature only in high iron doped ($n_{Fe2+} = 4 \times 10^{19}$cm^{-3}) ZnS crystals [6]. The absorption coefficient at these lines was $\sim$4% of the strongest ZPL absorption coefficient. Crystal field variations cause an inhomogeneous broadening of optical centers' transitions, which value does not depend on temperature. Hence, an inhomogeneous broadening could be estimated from the value of ZPL broadening measured at low temperature.

The ZPLs bandwidth in Cr and Fe doped ZnS, ZnSe crystals at low temperature were measured to be ~ 12 cm^{-1} or smaller for doping concentration on the order of 10^{19} cm^{-3} [2], [5], [6]. Therefore, aggregate center formation and inhomogeneous broadening are not substantial for RT laser applications when typical doping level of TM impurity is below 10^{19} cm^{-3}.

Spectroscopic properties of some chromium and iron doped II-VI materials are summarized in Table I.

B. Historical Background

1) Cr^{2+} Lasers: Due to the broad absorption band of Cr^{2+} ions in II-VI semiconductors spanning over the 1.3–2.1 μm spectral range a large variety of coherent sources have been successfully used for pumping of Cr:II-VI lasers. They include: Rare Earth doped fiber and solid state lasers (Er^{3+} @1.6 μm [34], [35], Tm^{3+} @1.9 μm [36], [46], Ho^{3+} @2.1 μm [37], [38]); TM doped solid state lasers (Co:MgF^2@1.9 μm [9], [39]); color center lasers ([40]); and Raman Shifted Nd^{3+} lasers [12], [39], [41]. The first lasing of a Cr:ZnSe crystal under direct pumping by InGaAsP/InP diode bars was reported in [42]. Later a 3.7 W CW diode pumped Cr:ZnSe laser was demonstrated in [43]. The progress in high power, reliable Er and Tm fiber lasers [28] has made them the most convenient and widely used pump sources for CW Cr^{2+} lasers. It is noteworthy that Cr:ZnSe/ZnS lasers could be pumped via photoionization transition by visible radiation. The Cr:ZnS/ZnSe oscillation under 532 nm pumping was reported in several publications [44], [45], albeit with low, less than 2%, pump efficiencies.

The first CW oscillation of Cr^{2+} lasers with output power of 250 mW with efficiency exceeding 60% was reported in 1999 [46]. 140 W of pure CW oscillation in Cr:ZnSe was achieved recently in [47]. Fig. 4 summarizes historical progress in development of high power CW lasers and shows that output power approximately doubled during a half-year period.

There are several important pulsed laser applications that require compact design with high output energy. A joule level MIR Cr:ZnSe laser pumped by free-running fiber-coupled Er-glass laser was recently reported in [59]. The maximum output energy of the Cr:ZnSe laser was measured to be 1.1 J. The output energy remains linear up to 6 ms pulse duration. A small roll-off due to thermal effects was observed for pulse durations longer than 7 ms.

Similar to the dye lasers, Cr^{2+} lasers effectively operate in a gain switched regime of oscillation with pulse duration in ns scale. Output energy of 20 mJ in 7 ns pulses from a single Cr:ZnSe oscillator operating at 10 Hz was demonstrated in [60]. A gain-switched Cr:ZnSe multi-stage MOPA system with output energy 52.2 mJ was recently reported in [61]. A brief review of the hybrid fiber-bulk (Er-fiber/Er:YAG, Tm-fiber: Ho:YAG/YLF) systems combining high efficiency of CW fiber lasers with high pulse energies of bulk materials and their use as pump sources of gain-switched Cr:II-VI lasers is provided below in Section II. The review of the gain switched Cr:ZnS/Se lasers operating at rep rate >100 Hz is presented in Section III.

Broad emission bands of TM:II-VI materials offer unique opportunities for generation of MIR ultra-short laser pulses. First Cr:ZnSe(ZnS) mode-locked lasers were demonstrated in [62]–[65]. A detailed review of mode-locked lasers based on chromium doped ZnS and ZnSe crystals is presented in Section III.

TABLE I
MATERIALS AND SPECTROSCOPIC PROPERTIES OF Cr^{2+} AND Fe^{2+} DOPED II-VI SEMICONDUCTORS (σ_{ab}, σ_{em},—PEAK ABSORPTION AND EMISSION CROSS-SECTIONS; λ_{ab}, λ_{em}—PEAK ABSORPTION AND EMISSION CROSS-SECTION WAVELENGTHS, RESPECTIVELY; $\Delta\lambda_{FWHM}$ –FULL BANDWIDTH AT HALF MAXIMUM; τ_{rad} RADIATIVE LIFE TAME; τ_{RT} (τ_{77K}) –LUMINESCENCE LIFETIME AT ROOM TEMPERATURE AND 77K; SECOND (d_{ij}) AND THIRD ORDER NONLINEAR OPTICAL SUSCEPTIBILITY (γ))

Host	ZnS	ZnSe	ZnTe	CdS	CdSe	CdTe
Physical properties [48]–[50]						
Crystal lattice*	ZB	ZB	ZB	W	W	ZB
Band Gap, eV	3.7	2.7	2.3	2.5	1.7	1.5
Bond length, Å	2.34	2.45	2.60	2.52	2.62	2.81
Max optical phonon ν, cm^{-1}	350	250	207	304	211	169
Thermal conductivity, W/cmK	0.27	0.18	0.108	0.2	0.09	0.075
Refractive index @3 μm	2.26	2.44	2.7	2.30	2.46	2.7
n^{-1} dn/dT, 10^{-5}**	1.9	2.6	6	4	4	4.4
Max d_{ij}, pV/m	12@1 μm	43@1 μm	119@1 μm	19@1 μm	65@1 μm	109@1 μm
γ at 1 μm, $\times 10^{20}$ m^2/W	84	~350	1200	500	150	3000
Spectroscopic properties of Cr^{2+} ions						
Peak $\sigma_{ab} \times 10^{-18}$ cm^2	1.0 [35]	1.1 [51]	1.2 [9]	1.5 [52]	1.9 [53]	2.2 [21]
Peak λ_{ab}, μm	1.69	1.77	1.79	1.85	1.92	1.92
Bandwidth $\Delta\lambda_{ab}$, μm	0.32	0.35	0.34	0.41	0.44	0.41
Peak $\sigma_{em} \times 10^{-18}$ cm^2	1.4 [35]	1.3 [51]	1.9 [9]	1.3 [52]	1.1 [54]	
Peak λ_{em}, μm	2.35	2.45	2.4	2.6	2.75	
Bandwidth $\Delta\lambda_{em}$, μm	0.82	0.86	0.87	1.1	1.2	
τ at RT, μs	4.3 [35]	5.5 [51]	3 [9]	1.2 [52]	3.7 [52]	2.9 [21]
τ_{rad}, μs	5.7 [35]	5.5 [51]	3 [9]	7.6 [52]	5.5 [52]	3.3 [21]
Spectroscopic properties of Fe^{2+} ions						
$\sigma_{ab} \times 10^{-18}$ cm^2	0.92 [6]	0.97 [32]			1.5 [55]	1.7 [56]
λ_{ab}, μm	2.8	3.1		3.15 [57]	3.5	3.65
$\Delta\lambda_{ab}$, μm	1.22	1.35		1.54 [57]	1.81	1.94
$\sigma_{em} \times 10^{-18}$ cm^2	1.1 [28]	1.1 [28]			3.2 [55]	1.4 [58]
λ_{em}, μm	3.94	4.35			4.81	5.94
$\Delta_{\lambda em}$, μm	0.91	1.13			1.37	1.79
τ at RT(77), μs	0.05(2.7) [31]	0.38 (57) [31]			0.05 [55]	0.24 (68) [58]
τ_{rad} RT, μs	55 [28]	57 [31]				72 [58]

*Zinc Blende (ZB) and wurtzite (W) crystal structure.
**Long-wavelength limit of temperature coefficient of the refractive index.

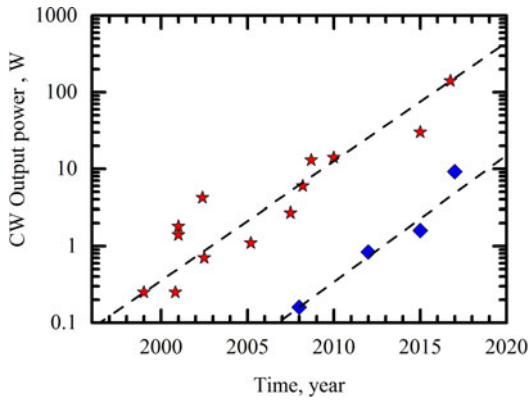

Fig. 4. Progress in high power CW TM:II-VI lasers: Cr^{2+}:ZnS/Se (stars), Fe^{2+}:ZnSe (squares). The dashed lines indicate exponential growth.

Tunable MIR lasing was demonstrated in several other Cr-doped binary, ternary and quaternary II-VI chalcogenides. The following chromium doped lasers have been described in the literature: Cr:CdSe (2.45–3.4 μm) [54], Cr:$Cd_{1-x}Mn_xTe$ (2.1–3.0 μm) [37], [66], Cr:CdTe (2.54 μm) [21], Cr:CdS (2.2–3.3 μm) [67], and Cr:ZnMgSe (2.3–2.7 μm) [68], [69]. The broadest tunability of a Cr:ZnSe laser covering 1.88–3.3 μm was demonstrated in [51], [70]. The longest wavelength oscillation of Cr^{2+} laser @3.6 μm was reported using a CdSe host [71]. Major milestones in Cr and Fe doped II-VI laser development are summarized in Table II.

2) Fe^{2+} Lasers: The first lasing of Fe^{2+} ions in tetrahedral sites was reported by Klein *et al.* [74] in 1983. The gain element was n-InP doped with iron and lasing was observed at 3.53 μm at 2 K. The first Fe:ZnSe laser pumped by 2.94 μm Er:YAG radiation and tunable over 3.98–4.5 μm spectral range was reported at T = 180 K [32]. The spectral position of Fe^{2+} absorption bands is around 2.5–4.0 μm where available pump sources are very limited. The following laser sources were used for excitation: Er^{3+} lasers operating at 2.9 μm [32]; Cr^{2+} laser operating over 2.6–2.9 μm [75]; D_2 Raman Shifted (2nd Stokes) Nd:YAG laser 2.92 μm radiation [76]; HF laser operating at 2.6 μm [79]. One of the ways to circumvent this limitation is to use energy transfer from other ions to create inversion of Fe^{2+} ions. Co^{2+} ions in II-VI semiconductors feature strong absorption bands near 0.8 μm and 1.5 μm and could be used for this application. Indeed, laser oscillation of Fe^{2+} ions in Co:Fe:ZnS(ZnSe) co-doped samples via energy transfer from cobalt was demonstrated under 790 nm and 1.56 μm pumping of Co^{2+} ions [80], [81]. Unfortunately, laser oscillation was realized only at low temperature (<24 K) due to overlapping of excited state absorption of Co^{2+} ions with Fe^{2+} luminescence band at higher temperatures.

TABLE II
MILESTONES IN DEVELOPMENT OF Cr^{2+} AND Fe^{2+} LASERS

Milestone		Ref.
Cr^{2+} lasers		
First lasing	1996	[9]
First diode-pumped laser	1997	[42]
First CW laser	1999	[72]
First mode-locked laser	2000	[62]
First Kerr mode-locked laser	2009	[73]
Gain element:	*Tunability*	
Cr:ZnS	1.84–3.06 μm	This paper
Cr:ZnSe	1.88–3.30 μm	[51], [70]
Cr:CdSe	2.26–3.61 μm	[71]
Fe^{2+} laser		
First lasing of Fe^{2+} ions	1983	[74]
First lasing in chalcogenide host	1999	[32]
First CW lasing	2008	[75]
First RT lasing	2005	[76]
Gain element:	*Tunability*	
Fe:ZnS	3.49–4.65 μm	[77]
Fe:ZnSe	3.77–5.05 μm	[26]
Fe:CdSe	4.60–6.10 μm	[78]

Highly efficient laser oscillations of Fe:ZnS(ZnSe) pumped by free running 2.94 μm Er^{3+} laser radiation were demonstrated at temperatures of 77–220 K by several research groups [82]–[84]. Recently, a 5 J pulsed Fe:ZnSe laser operating at T = 85 K and pumped by a free running 10 J Er:YAG laser was reported in [85].

The first CW lasing of Fe:ZnSe pumped by 2.97 μm Cr^{2+}:CdSe laser radiation was demonstrated in [75]. The authors reported 160 mW of output power at 4 μm wavelength. Current progress in development of high power Cr^{2+} CW lasers enabled power scaling of Fe:ZnSe output power in excess of 9 W [86]. Fig. 4 shows progress in development of CW Fe^{2+} lasers. As one can see from the figure, the exponential growth rates for the output power of Fe^{2+} and Cr^{2+} lasers are very similar.

The first RT operation of an Fe:ZnSe laser was proposed and realized in [76]. The authors demonstrated that Fe:ZnS/ZnSe crystals could efficiently operate at RT in the gain-switched regime of operation if the pump pulse duration is shorter than, or of the same order of magnitude as, the quenched lifetime of Fe^{2+} optical centers at RT. Recent progress in RT Fe^{2+} lasers strongly correlates with the development of high-energy pump sources based on solid-state lasers and HF chemical laser. A highly efficient Fe:ZnSe laser with an output energy of 1 J pumped by an HF laser operating at 20 Hz was demonstrated in [87]. The output energy of the Fe:ZnSe laser reached 1.4 J in $\sim$150 ns pulse duration when pumped by HF laser radiation in single pulse regime [88]. In our review we will mainly focus on Fe:ZnSe laser systems pumped by solid state lasers.

Table II also summarizes tuning ranges of Fe^{2+}:II-VI lasers. The shortest 3.49 μm oscillation wavelength was demonstrated using ZnS hosts [77]. The longest 6.1 μm was achieved in CdSe crystals [26], [55].

TABLE III
PROPERTIES OF ER:YAG, HO:YLF, AND HO:YAG [48], [90]

Property	Er:YAG	Ho:YLF	Ho:YAG
Crystal type	Isotopic	Birefringent	Isotopic
Central wavelength λ_c, nm	1645	2051	2090
Pump wavelength λ_p, nm	1470/ 1532.6	1940	1908
Thermal conductivity, Wm/K	13	6.3	13
Peak emission cross-section σ_e, 10^{-20} cm^2	2.7	1.81	0.98
Lifetime τ, ms	5	15	7
Thermal coefficient of refractive index (dn/dT), 10^{-6} K^{-1}	7.8	-4.3 (//c) -2.0 ($\perp$c)	7.3

II. TM:II-VI LASERS PUMP SOURCES BASED ON HYBRID, FIBER-BULK SYSTEMS

A. Introduction

Er and Tm fiber lasers [28] are the most convenient and widely used pump sources for CW Cr^{2+} lasers. The review of these fiber lasers is out of the scope of the current paper and can be found elsewhere [89]. This section is focused on recent developments in Q-switched fiber-bulk hybrid lasers combining effective operation of fiber lasers in CW regime and energy storage capability of solid state lasers. These systems are used as pump sources for TM:II-VI lasers operating in the gain-switched regime. In addition, these hybrid laser sources operating in the eyesafe wavelength regions have a variety of applications in medicine, range-finding, remote sensing, and industrial material processing. Due to the broad availability of high-brightness fiber laser optical pump sources, the most attractive are the eyesafe solid-state laser systems based on resonantly-pumped Ho:YAG (pumped by Tm-doped fiber laser (TDFL) at 1908 nm), Ho:YLF (pump by Tm-doped fiber lasers at 1940 nm), and Er:YAG (pumped by Er-doped fiber lasers (EDFL) at 1532 nm) laser gain media. Thermal, optical, and spectroscopic parameters of Er:YAG and Ho:YAG/YLF are summarized in Table III. Due to long storage lifetime and high peak emission cross section, these lasers efficiently convert CW radiation of the fiber pump sources into high-energy, high peak power pulsed oscillators and deliver high quality, high-brightness laser beams at 2090 nm, 2050 nm, and 1645 nm, respectively. These properties open an excellent opportunity for obtaining high energy MIR radiation via optical parametric oscillators (OPOs) and direct pumping of transition metal doped II-VI semiconductor materials.

Systems such as Er:YAG lasers at 1645 nm are preferable for direct pumping of Cr^{2+}:ZnS gain medium whereas Ho:YLF/ Ho:YAG lasers at 2050/2090 nm are more suitable for Cr^{2+}:ZnSe gain material pumping.

B. Fiber Pumped Er:YAG Laser

Er:YAG lasers with emission at 1645 nm and 1617 nm have been realized by in-band pumping by EDFL [91]–[93]. High energy generation under laser diode pumping has been reported in [94], [95]. Obtaining high energy Er:YAG lasers operating at

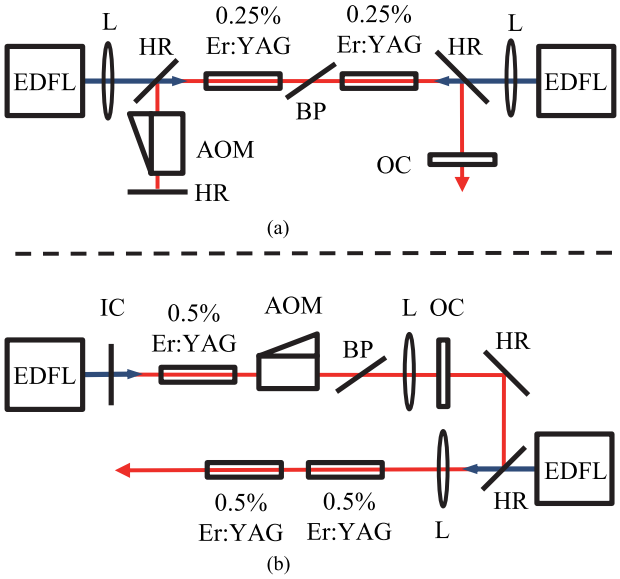

Fig. 5. Resonator schematic of high energy Er:YAG oscillator optimized for (a) low repetition rates (<5 kHz) and (b) high repetition rate (>5 kHz) MOPA: EDFL, pump laser at 1532 nm; L, pump focusing lens; Er:YAG, gain element; HR, high reflectors; AOM, Acousto-optic modulator; BP, Brewster plate; OC, output coupler; EDFL – Er fiber laser. The pump beam size in all cases is ~1.2 mm. In the MOPA system the output beam of the Er:YAG master oscillator was collimated to match the pump beam diameter before focusing into the gain elements of the amplifier.

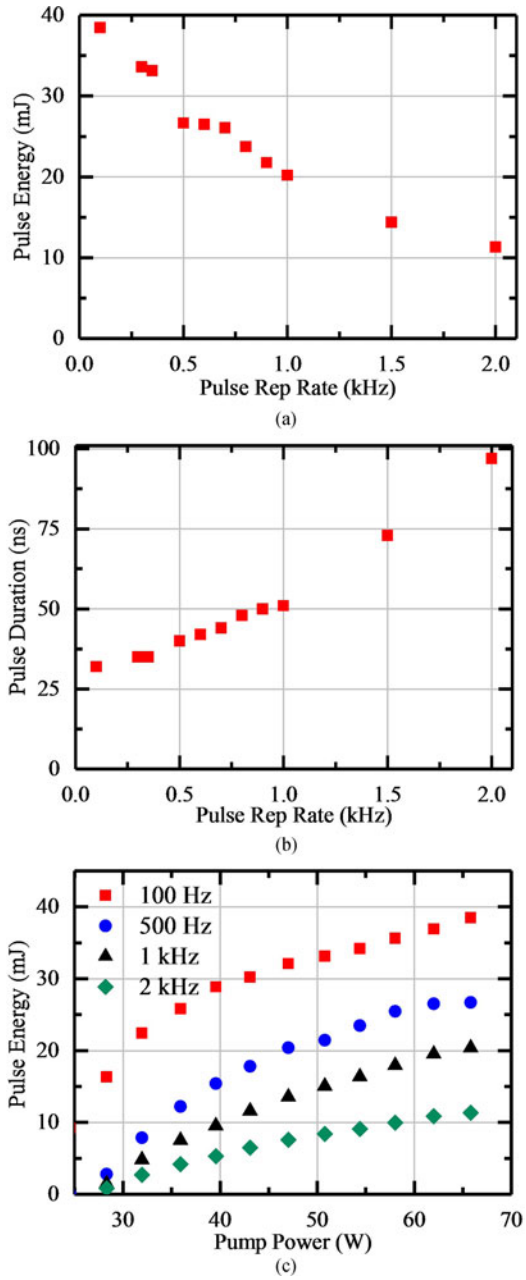

Fig. 6. Output characteristics of low repetition rate Er:YAG oscillator (<5 kHz) design. Pulse energy (a) pulse duration (b) of Er:YAG Q-switched lasers vs a pulse repetition rate. (c) Output pulse energy as a function of incident pump power for different repetition rates.

1 kHz, however, has proven to be a challenging task. Here, we present two designs of high energy 1645 nm lasers suitable for operating at low (<5 kHz) and high repetition rates (>5 kHz).

Previous attempts of hybrid Er:YAG laser operating at ~1 kHz were limited by damage to dielectric coatings of the input mirror [93]. Our approach, which is tailored to operate at low repetition rates, is depicted in Fig. 5(a). The master oscillator (MO) was composed of two 1532.6 nm, 30 W EDFLs and a resonator based on two 5 mm diameter by 60 mm long 0.25% doped Er:YAG crystals. The beam was passed through high reflection (1645 nm)/high transmission (1532.6 nm) dichroic mirrors and Q-switched operation was achieved by Gooch & Housego acousto-optic modulator (AOM). A volumetric Bragg grating (VBG) with an effective reflection of 65% at 1645 nm served as an output coupler. The cavity length was optimized such that the beam size at the input mirrors and crystals is ~0.8 mm ($2w$) allowing maximized extraction of energy without laser-induced damage of components. Fig. 6 summarizes output characteristics of the low repetition rate Er:YAG laser design. At full power pumping (64 W) we demonstrate 22 mJ, 50 ns pulses operating at 1 kHz. Output energy of 40 mJ at <100 Hz was limited by optical damage of the antireflection (AR) coating on the VBG. Further improvement of output characteristics can be achieved by 1) improving AR coating on the VBG, and 2) use of high power pump sources (>100 W EDFL).

Fig. 5(b) depicts the design of a high average power, high repetition rate Er:YAG laser. It is a MO and power amplifier (MOPA) configuration employing two 30 W EDFLs. The master oscillator is based on one EDFL pumping one 5 mm diameter by 40 mm long 0.5% Er:YAG crystal. The cavity consists of a dichroic input mirror (IM), a crystal, AOM, a Brewster etalon, an intracavity lens, and a VBG with a 65% reflection. The generated light is then passed through a single pass power amplifier consisting of two 40 mm long 0.5% Er:YAG crystals pumped by a second 30 W EDFL. Output characteristics are summarized in Fig. 7. Here, output energies of up to 2.6 mJ were achieved at 10 kHz rep. rate. Average output power of high repetition rate MOPA Er:YAG did not exceed 26 W for the whole range of repetition rates 5–100 kHz. Further Er:YAG energy scaling can be achieved by the use of higher power EDFL pump sources.

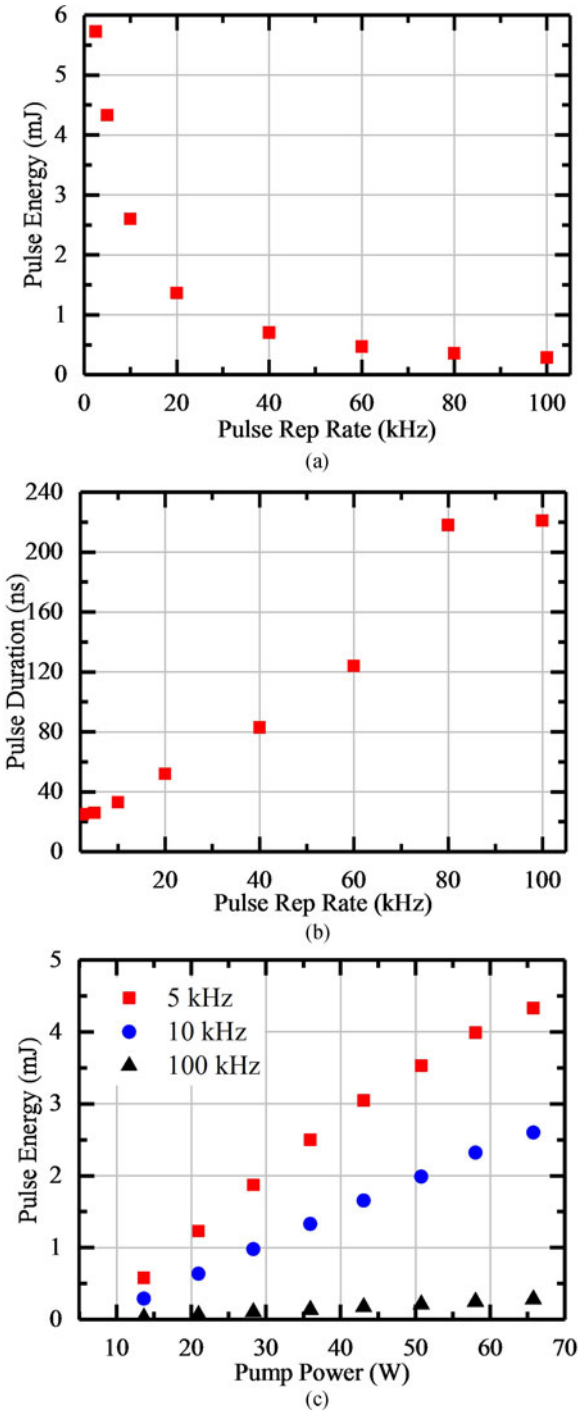

Fig. 7. Output characteristics of high repetition rate MOPA Er:YAG (>5 kHz) laser design. Pulse energy (a) pulse duration (b) of Er:YAG Q-switched lasers vs a pulse repetition rate. (c) Output pulse energy as a function of incident pump power for different repetition rates.

C. *Fiber Pumped Ho:YAG Laser*

Direct resonant pumping of Q-switched Ho:YAG lasers by TDFL lasers operating at 1908 nm allows for obtaining high energy nanosecond pulsed output radiation at 2.09 μm at pulse repetition rates ranging from tens of Hz to hundreds of kHz with high optical to optical efficiencies. A very important application of fiber-pumped Q-switched Ho:YAG lasers is pumping

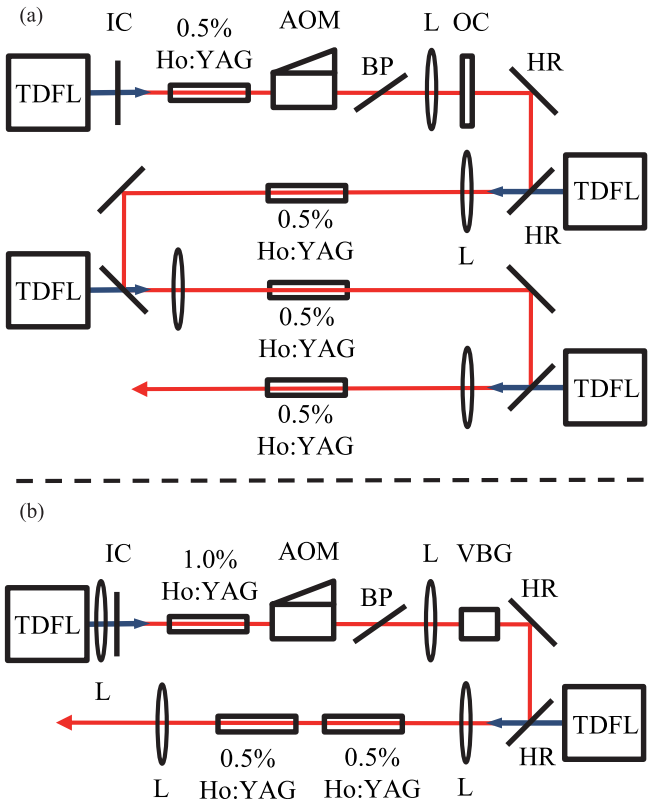

Fig. 8. MOPA schematic of high energy (a) and high rep rate (b) Ho:YAG lasers: TDFL – Tm fiber pump laser at 1908 nm; L – lens, HR – dichroic high reflectors (AR@1908 nm, HR@2090 nm); AOM – Acousto-optic modulator; BP – Brewster plate; OC – output coupler; VBG – volumetric Bragg grating. The pump beam size in all cases is ~2.3 mm. In the MOPA system the output beam of the Ho:YAG master oscillator was collimated to match the pump beam diameter before focusing into the gain elements of the amplifier.

of Cr:ZnSe gain crystals in gain-switched laser configuration. This approach allows for obtaining 10 ns pulses in the spectral range of 2–3 μm (see Section III).

High energy Ho:YAG systems with high optical efficiencies were studied extensively [96]–[98]. In general, the efforts of power scaling are limited by strong thermal lensing in Ho:YAG crystals resulting in permanent optical damage of dielectric coatings within the cavity. Here, we present our latest achievement in power scaling of Ho:YAG lasers. General optical diagrams of high-energy and high pulse repetition rate systems are shown in Fig. 8. In the case of high-energy systems, the cavity is optimized for larger active volume in the Ho:YAG gain elements and larger spot sizes to minimize optical damage. This leads to lower optical-to-optical efficiency but allows for obtaining very high pulse energies at low pulse rep rates (up to 1 kHz). In contrast, high rep-rate systems are optimized for maximum possible gain. Thus we use relatively tight pump focusing, small mode diameter, and higher Ho concentration. This approach enables shortening of the pulse duration at high pulse rep rates (e.g., 100 kHz).

The high-energy system was composed of four stages: a MO and 3-stage power amplifier (PA), and is depicted in Fig. 8(a). Two 100 W TDFLs operating at 1908 nm and split with 50/50 beam splitters were used to pump each channel. The MO

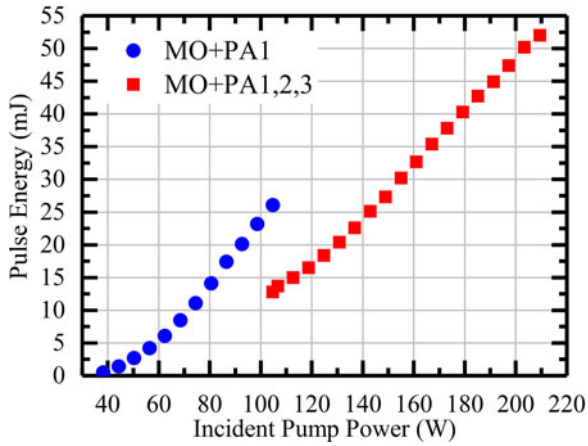

Fig. 9. Output pulse energy characteristics of low repetition rate (1 kHz) Ho:YAG oscillator design as a function of incident pump power. Blue curve (circles) represents output energy from Master Oscillator and first amplifier stage (PA1) simultaneously pumped by the first 100 W TDFL. Red curve (squares) represents MOPA passed through second and third amplifier (PA2 PA3) stages simultaneously pumped by the second 100 W TDFL.

consisted of one input coupler (IC), an intracavity lens (to compensate thermal lens in MO gain element), a 5 mm diameter by 40 mm long 0.5% Ho:YAG crystal, AOM, a Brewster etalon and a R = 40% output coupler. The MO output energy at 2090 nm was 14.5 mJ with pulse duration of 17 ns. Each consecutive amplifier stage was composed of a single 40 mm long 0.5% Ho:YAG crystal and mode matched with pump by a long focal length lens. The resultant output energy after each stage was as follows: PA1 – 25 mJ, PA2 – 34 mJ, PA3 – 52 mJ retaining the pulse duration of 17 ns (Fig. 9). Our further efforts for power scaling will include a new and improved design of the MO based on Er:YAG schematic introduced in Section II-B.

The high rep-rate system shown in Fig. 8(b) was also built using a MOPA approach. The pump beam is tightly focused into 1.0% gain element of the MO and the cavity is made as short as possible. To reduce the pulse duration and ensure narrow-linewidth at 2090 nm, a low-efficiency VBG is used as the output coupler. The output beam of the MO is then focused together with the second pump beam into a dual-crystal 0.5% Ho:YAG single-pass amplifier gain element. The output characteristics of the high rep-rate system are summarized in Fig. 10.

D. Fiber Pumped Ho:YLF Laser

Ho:YLF as the gain medium features a combination of a high gain cross-section and long storage time of the Ho-transition as well as birefringent and athermal nature of the YLF crystal essential in the design of high-power linearly polarized laser systems. As with Ho:YAG, Ho:YLF laser system design is well suited for a pumping scheme utilizing randomly-polarized, high-brightness Tm-fiber lasers but with a small difference in design. In this case it is convenient to polarization-split the fiber laser output into two independent pump channels which can be used to pump two laser crystals. In our case we use one channel to pump a crystal in a laser oscillator and the other channel to pump a crystal configured as a single-pass amplifier. This dual-crystal MOPA approach is described in [99], [100]. The Tm-fiber lasers

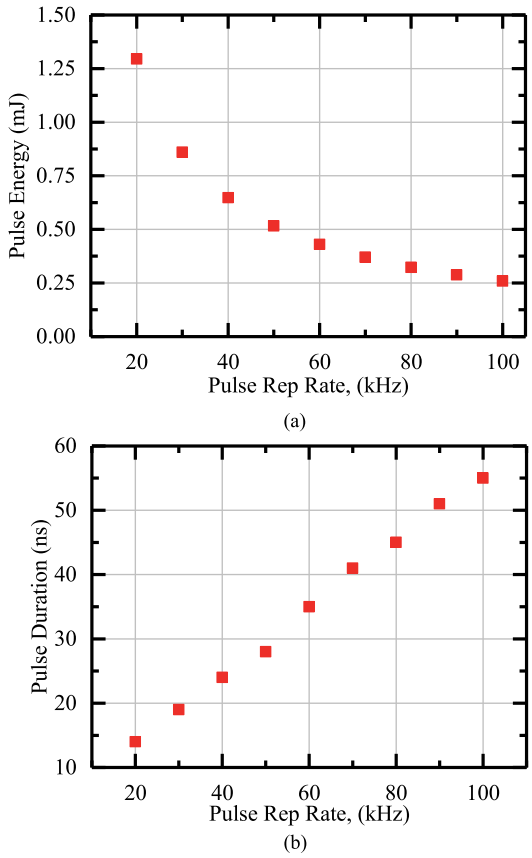

Fig. 10. (a) Pulse energy vs repetition rate of high repetition rate Ho:YAG oscillator (b) Pulse duration vs repetition rate of high repetition rate Ho:YAG oscillator.

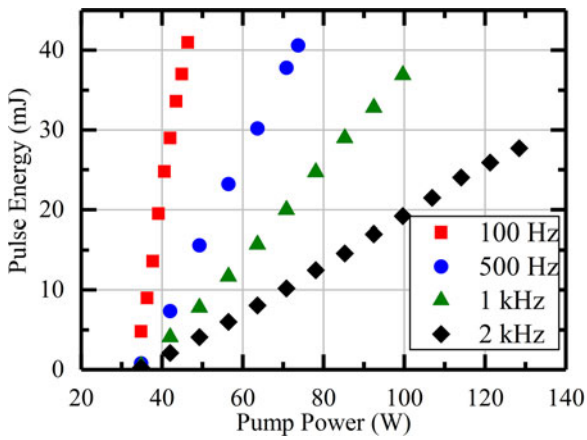

Fig. 11. Ho:YLF MOPA output pulse energy in Q-switched regime at various repetition rates.

for pumping Ho:YLF lasers are typically operated at 1940 nm and produce ~100–150 W in CW regime with diffraction-limited beam quality. The performance of the Ho:YLF MOPA system is illustrated in Fig. 11. The absolute optical-to-optical efficiency reaches ~47% in CW regime. Fig. 11 illustrates the output pulse energy in Q-switched regime at different repetition rates vs total Tm-pump power. No alignment or optimization was performed on the system while recording the data in Fig. 11. Typical pulse width for the Ho:YLF MOPA is

~15–17 ns while operating at pulse energies >35 mJ. The addition of a dual-crystal Ho:YLF single-pass amplifier after the MOPA enables a 2-fold improvement in energy, i.e., >70 mJ at 1 kHz, and >100 mJ at <500 Hz [100].

III. High-Power Middle-IR Sources Based on Polycrystalline Cr:ZnS and Cr:ZnSe

A. Introduction

During recent years we have observed a rapidly growing popularity of CW MIR laser sources operating within the 2–3 μm spectral region. Our MIR laser systems are based on Cr^{2+}:ZnS and Cr^{2+}:ZnSe gain media capable of delivering high-power, high-brightness CW laser radiation in the spectral range of 1800–3400 nm [70], [101]. These lasers have been used for a broad variety of applications that include, but are not limited to, precision laser spectroscopy, detection of organic compounds, defense applications, and medical research. There is also a rapidly growing demand for very high-power, high-brightness mid IR laser systems (more than 100 W, high beam quality) in the fields of industrial material processing for fast cutting, welding, and marking of polymers near 2400 nm wavelength region, processing of glasses in the range of 2700–2950 nm, manufacturing of biomedical equipment products, and laser surgery near 2940 nm. In this section we review our recent progress in development of state-of-the-art MIR Cr^{2+}:ZnS and Cr^{2+}:ZnSe lasers and demonstrate their unique output characteristics.

B. Widely Tunable Cr:ZnS and Cr:ZnSe Lasers

The availability of high-power fiber lasers operating in the 1.5–1.9 μm spectral range which deliver near diffraction-limited beam quality has enabled significant progress in development of reliable widely-tunable, narrow-linewidth, and single-frequency MIR Cr^{2+}:ZnS and Cr^{2+}:ZnSe laser systems [28]. Cr^{2+}:ZnS/Se tunable lasers deliver more than 8 W of output power at the central wavelength and more than 1000 nm continuous tunability, while maintaining <0.25 nm laser linewidth and high beam quality. The single-frequency systems reach 5 W output power level and up to 500 nm tuning range (tunability of the single-frequency lasers is currently limited by bandwidth of diffraction gratings operating in low-efficiency Littman configuration). Fig. 12 shows general optical diagrams of the tunable Cr^{2+}:ZnS and Cr^{2+}:ZnSe lasers in MOPA configurations. Fig. 13 depicts typical tuning curves of narrow-line and single-frequency Cr^{2+}:ZnS lasers.

C. Power-Scaling CW Cr:ZnS and Cr:ZnSe Lasers With Spinning-Ring Gain Element Approach

Due to inherent physical properties of ZnS and ZnSe hosts, the maximum output power of Cr^{2+}:ZnS and Cr^{2+}:ZnSe lasers was limited to about 10 W [28]. The primary limiting factors for power scaling of these laser systems are extremely strong thermal lensing [102] and relatively low optical damage threshold [103], [104]. In order to mitigate these challenges and significantly increase achievable output power of Cr^{2+}:ZnS and Cr^{2+}:ZnSe CW laser systems we have recently developed a

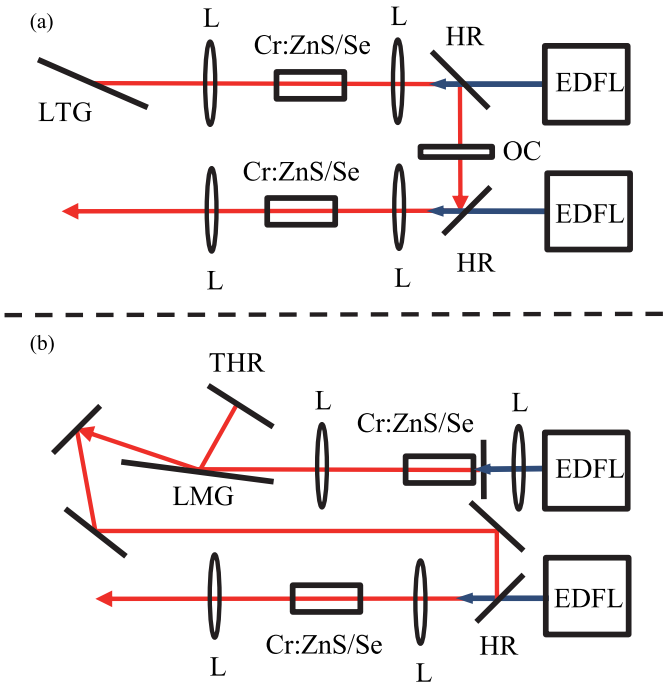

Fig. 12. General optical scheme of CW widely tunable narrow-line (a) and single-frequency (b) Cr^{2+}:ZnS and Cr^{2+}:ZnSe lasers in MOPA configurations. EDFL – fiber pump laser; HR – dichroic mirror (HR@2000–3000 nm, AR@1500–1700 nm); L – AR-coated lens; LTG – diffraction grating in Littrow mount configuration; LMG – diffraction grating in Littman mount configuration; THR – tuning high reflector; OC – output coupler. Depending on the output power requirements, the MOPA systems may use either dual or single pump laser (with 50/50 pump beam splitting in the latter case). Cr:ZnS is preferable for higher output powers at shorter wavelengths, while Cr:ZnSe is more suitable for longer wavelengths. A combination of Cr:ZnS and Cr:ZnSe in the master oscillator and power amplifier, respectively, allows for achieving a broader wavelength tuning range. The pump beam size in all cases is ~1.2 mm, the master oscillator typically delivers ~1.5 mm output beam. No special beam shaping of the master oscillator is used in these systems. The typical length of the gain elements is 9 mm with Cr concentration of 5×10^{18} cm^{-3}.

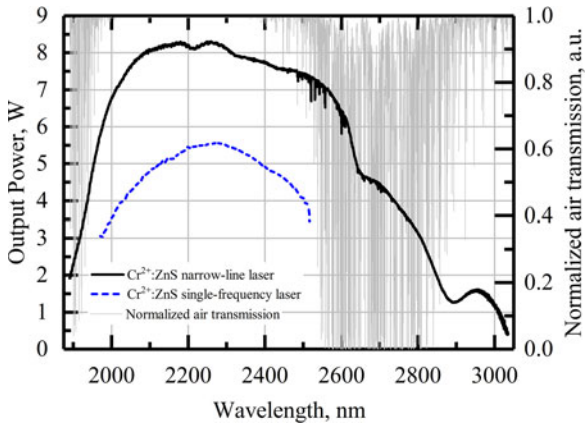

Fig. 13. Continuous wavelength scan of a tunable Cr^{2+}:ZnS MOPA. Grey background plot (right y-axis) shows calculated standard air transmission through 0.5 m optical path (roughly corresponds to 10 cavity roundtrips). Solid line plot (left y-axis) shows a wavelength scan under continuous cavity purging with dry high-purity Nitrogen gas. When the laser wavelength is tuned close to strong atmospheric absorption lines, severe intracavity losses lead to significant power drops. Cavity purging results in significant suppression of intracavity losses and restores the laser output power. The residual atmospheric absorption is still detectable in the 25 mm air path between the laser and power meter. The dashed plot shows a typical tuning curve of the single-frequency Cr^{2+}:ZnS MOPA laser system.

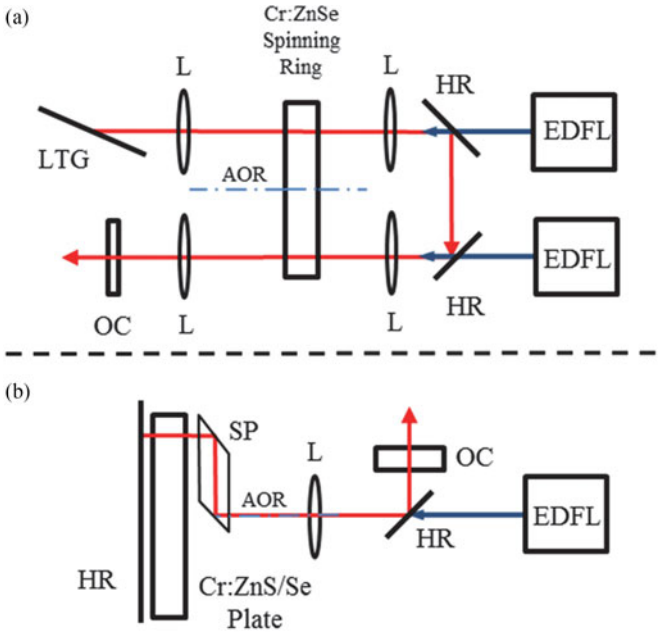

Fig. 14. Generic optical diagrams of the spinning-ring gain element (a) and spinning-cavity (b) Cr^{2+}:ZnS and Cr^{2+}:ZnSe laser systems. EDFL – fiber pump laser; HR – dichroic mirror (HR@2000–3000 nm, AR@1500–1700 nm); L – AR-coated lens; LTG – diffraction grating in Littrow mount configuration; SP - spinning periscope; AOR – axis of rotation of the ring gain element (a) or the spinning periscope (b); OC – output coupler.

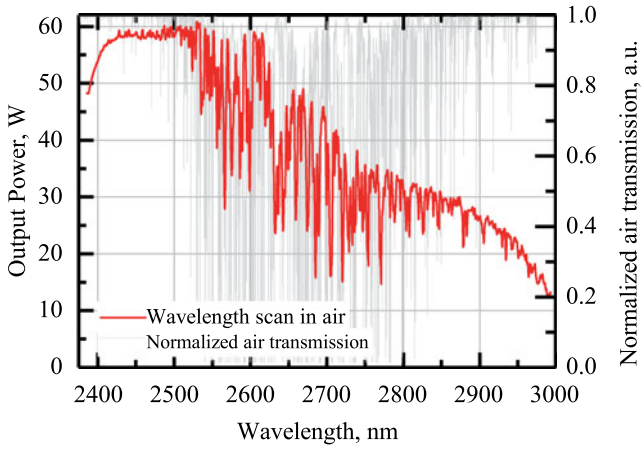

Fig. 15. Continuous wavelength scan of a tunable Cr^{2+}:ZnSe spinning-ring master oscillator. Grey background plot (right y-axis) shows calculated standard air transmission through 0.5 m optical path (approximately 0.5 cavity round trips).

novel approach which consists of a rapid scanning of coaxial pump beam and laser mode through the gain element. In the simplest implementation the Cr^{2+}:ZnS or Cr^{2+}:ZnSe gain element is manufactured in the form of a ring which is spinning in the laser cavity at high RPM. This approach allows us to completely eliminate thermal lensing effects due to a very low local heating, avoid optical damage of the gain element, and thereby obtain record levels of output power limited only by the available pump.

A very detailed description of this laser system can be found in [47] and a generic optical diagram of the spinning ring laser is shown in Fig. 14(a). An alternative optical scheme which uses exactly the same principle of operation is depicted in Fig. 14(b). In the latter system, the gain element is made in the shape of a plane-parallel plate (this can be either of circular or rectangular shape) and the coaxial pump beam and laser mode are scanned through the gain element on a circular path using a spinning periscope consisting of a single piece of IR optical material or a pair of parallel mirrors. We designate this design of the system as "spinning cavity" laser.

The main advantage of the spinning ring over spinning cavity is that multiple pump sources can be used simultaneously: using two 100 W, 1.9 μm Tm fiber lasers we were able to obtain 140 W of output power at 2.4 μm and 30 W at 2940 nm [47] and we expect to reach at least 250 W maximum output power level with 4 such pump sources from a single gain element. On the other hand, self-cooling of the spinning ring has somewhat limited heat removal efficiency and becomes challenging from an engineering perspective. In contrast, in the spinning cavity design the gain element plate is fixed on a heatsink that allows for efficient heat removal using conventional cooling methods (e.g., water cooling). The greatest disadvantage of the spinning cavity design is that only one pump source can be used, therefore requiring very high power pump sources. In our preliminary experiments we obtained about 50 W of output power near 2.4 μm at 100 W incident pump power. Nevertheless, with continuing progress in fiber laser technology this problem might be soon mitigated as kW level high-brightness fiber pump lasers become available, allowing for further progress in power scaling of MIR laser systems based on Cr^{2+}:ZnS and Cr^{2+}:ZnSe gain media. Also, currently under consideration is the feasibility of using multimode fiber pump sources.

To conclude this section, we present our most recent results in tunability of the spinning-ring Cr^{2+}:ZnSe laser system. The tuning curve of the laser is shown in Fig. 15. The tuning range was limited by dichroic mirrors while the maximum output power was limited by the damage threshold of the diffraction grating. To mitigate these problems in the future, we are currently developing a MOPA system where in place of the master oscillator we will use our mid-power widely tunable Cr^{2+}:ZnS laser system (Figs. 12 and 13) and the spinning ring will be used as a dual-pass power amplifier.

D. Gain Switched Cr:ZnS/ZnSe Lasers

A general diagram of a tunable gain-switched (GS) Cr:ZnS/Se laser is shown in Fig. 16. We used Q-switched Er:YAG / Ho:YAG laser operating at 1645 nm/2090 nm as a pump source (see Section II for details). The cavity consisted of a high reflection folding mirror with R $>$ 99%, a gain crystal with antireflection coatings on both facets, output coupler with R $=$ 50%, and a high efficiency ($>$90%) diffraction grating placed in Littrow configuration for wavelength tuning. A dual prism beam expander was inserted to 1) provide narrow laser linewidth and 2) prevent optical damage of the diffraction grating.

For the Cr:ZnSe laser, a Ho:YAG pump laser was assembled operating at 100–200 Hz repetition rates with pulse energy over 30–55 mJ range and 30 ns pulse duration. Output characteristics

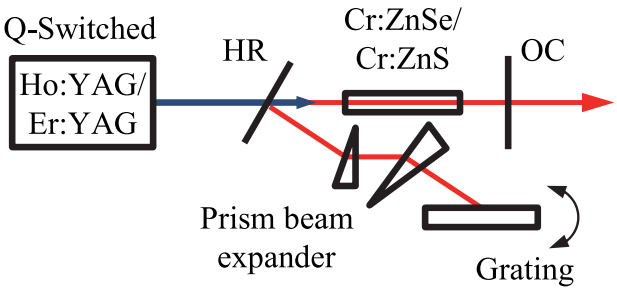

Fig. 16. Schematic of tunable gain switched Cr:ZnS/Cr:ZnSe laser.

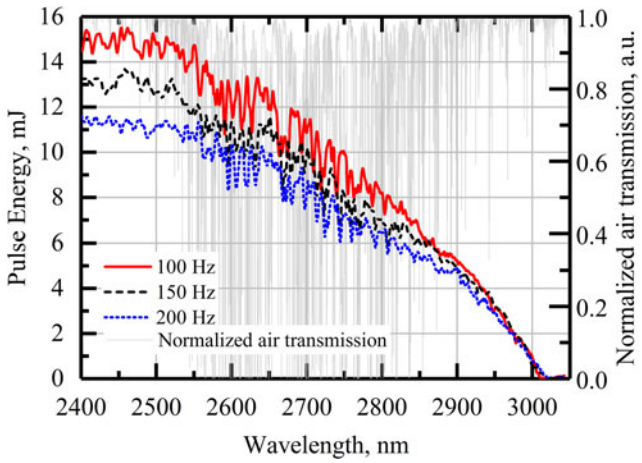

Fig. 17. Tuning curves of tunable gain switched Cr:ZnSe laser at different frequencies of operation: (i) 100 Hz, (ii) 150 Hz, (iii) 200 Hz. Sharp dips at 2550–2850 nm are due to intracavity atmospheric water vapor absorption. Gray background shows the transmission of 1 m standard air.

of the GS Cr:ZnSe laser are shown in Fig. 17. We achieved wavelength tuning over 2400–3000 nm with maximum output energy as high as 16 mJ at the 2500 nm peak. Pulse duration was 10 ns.

For the Cr:ZnS laser, a dual Er:YAG pump laser was assembled operating at 100 Hz repetition rate with pulse energy of 12 mJ and 80 ns pulse width. Pumping was performed at Brewster angle from both sides of the crystal. Output characteristics of the GS Cr:ZnS laser are shown in Fig. 18. We achieved wavelength tuning over 1950–2650 nm with output energy as high as 7 mJ at the 2250 nm peak. Pulse duration was 50 ns.

IV. Ultrafast Middle-IR Sources Based on Polycrystalline Cr:ZnS and Cr:ZnSe

A. Introduction

Our review of this topic will be organized as follows. The most current designs and output parameters of polycrystalline Cr:ZnS and Cr:ZnSe oscillators are summarized in Section B. Recent results on amplification and spectral broadening of MIR fs pulses in single-pass polycrystalline Cr:ZnS and Cr:ZnSe amplifiers are discussed in Section C. We conclude the review with a short summary on the down-conversion of Cr^{2+}-based fs sources in synchronously pumped optical parametric oscillators (OPOs).

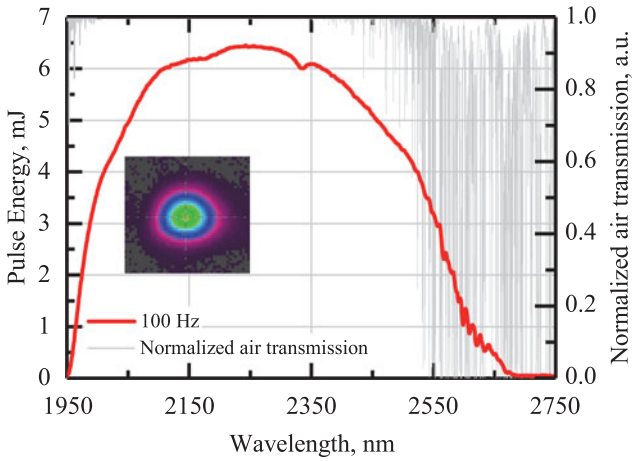

Fig. 18. Tuning curves of tunable gain switched Cr:ZnSe laser operating at 100 Hz. Insert is the laser beam profile. Gray background shows the transmission of 1 m standard air.

TABLE IV
Properties of Cr:ZnS, Cr:ZnSe, and Ti: Sapphire

Property	Cr:ZnS	Cr:ZnSe	Ti:Sa
Central wavelength λ_C, μm	2.35	2.45	0.8
Relative bandwidth $\Delta\lambda/\lambda_C$	0.6	0.6	0.6
Bandwidth $\Delta\nu$, THz	70	70	130
Peak emission cross-section σ_e, 10^{-19} cm^2	14	13	4
Nonlinear index n_2, cm$^2\cdot$W^{-1}	10^{-14}[b]		$3\cdot10^{-16}$
Second order nonlinear susceptibility $\chi^{(2)}$, pm$\cdot$V^{-1}	4[b]	16–20[b]	Very low
[a]Lifetime τ, μs	4.3	5.4	3
[a]Thermal conductivity, W$\cdot$m$^{-1}\cdot$K^{-1}	27	18	35
[a]Temperature derivative of refractive index (dn/dT), $10^{-6}\cdot$K^{-1}	54	61	12
Hardness, Mohs	4	4	9

[a]At room temperature (RT).
[b]Approximate values.

Chromium doped ZnS and ZnSe are well suited for generation of ultra-short optical pulses in the MIR range. These materials combine superb ultra-fast laser capabilities with high nonlinearity of wide-bandgap zinc-blende semiconductors. Therefore, Cr:ZnS and Cr:ZnSe support all standard regimes of femtosecond (fs) lasers and amplifiers and also enable efficient frequency conversion of ultra-short pulses via $\chi^{(2)}$ and $\chi^{(3)}$ nonlinearity.

Due to their broad absorption and emission bands, Cr:ZnS and Cr:ZnSe are often referred to as the "Ti:sapphire of the middle-infrared". Relevant properties of the materials are compared in Table IV. As can be seen, Cr:ZnS and Cr:ZnSe exhibit significantly higher peak emission cross-section and longer RT lifetime at similar relative bandwidth. On the other hand, Cr:ZnS and Cr:ZnSe are more demanding in terms of the thermal management due to smaller thermal conductivity, higher temperature derivative of refractive index and lower hardness.

Convenience of RT operation and availability of high power fiber lasers for optical pumping have stimulated rapid progress of ultrafast Cr:ZnS/Se lasers. Femtosecond oscillators based on all

major mode-locking techniques have been implemented over the past decade. Passive mode-locking of single-crystal Cr^{2+}:ZnSe lasers by a semiconductor saturable absorber mirror (SESAM) with $\sim$100 fs pulses was demonstrated in 2005 [105], [65]. Kerr-lens mode-locking of a single-crystal Cr:ZnSe laser with 95 fs pulses was achieved in 2009 [73]. The first Cr:ZnSe-based chirped-pulse amplifier (CPA) with sub-mJ pulse energy and GW peak power was demonstrated in 2011 [106]. A graphene mode-locked single-crystal Cr:ZnSe laser (226 fs pulses) was first reported in 2013 [107].

Further efforts of several research teams were concentrated on the improvements of Cr-based oscillators and amplifiers, as reviewed in [108]. Optimization of SESAM mode-locked oscillators has allowed the achievement of 50 fs pulses at 0.25 W average power (and implementation of a kHz CPA with 5 GW peak power) [109]. Pulse durations as short as 41 fs (5 optical cycles) and repetition rates as high as 0.95 GHz were obtained from single-crystal Cr:ZnS lasers passively mode-locked by graphene [110], [111]. However, it was understood that the use of SESAM and Graphene mode-lockers imposes limits on further power scaling of Cr-based fs oscillators [108], [112]. On the other hand, optimization of the single-crystal Kerr-lens mode-locked Cr:ZnS and Cr:ZnSe lasers resulted in $<$70 fs pulses, and has allowed the realization of sub-W levels of output power [113]–[115].

All recent developments in ultrafast Cr-based laser technology are related to Kerr-lens mode-locking in polycrystalline Cr:ZnS and Cr:ZnSe, which was first achieved in 2014 [116]. The use of optimized polycrystalline gain elements and unconventional designs of the optical resonators has resulted in significant improvements in the output parameters of MIR fs oscillators in terms of average power, pulse energy, and pulse duration [28]. The most current achievements include 2–3 optical-cycle oscillators with Watt-level average power and MW-level peak power [117]–[119]. Efficient power scaling of ultra-fast MIR oscillators in simple and robust single-pass polycrystalline Cr:ZnS and Cr:ZnSe amplifiers has been demonstrated, resulting in few-optical-cycle MIR sources with multi-Watt (multi-MW) average (peak) powers which operate in very broad range of pulse repetition rates [120], [121].

Another set of interesting opportunities arises from the high nonlinearity of zinc-blende semiconductors. Nonlinear refractive indices of ZnS and ZnSe are approximately 30–50 times higher than that of sapphire (see Table IV); the critical power for self-focusing in these materials is proportionally low ($P_{\mathrm{Crit}} \approx 0.4$ MW at the wavelength 2.4 μm). Filamentation and supercontinuum generation (SCG) in bulk ZnS and ZnSe attracts growing attention from the ultrafast laser community. The formation of filaments and multi-octave MIR SCG has been recently investigated in undoped ZnS and ZnSe [122]–[126]. The parameters of filaments were characterized in a broad range of pump wavelengths (and hence in different regimes of multi-photon ionization) using MIR optical parametric amplifiers (OPA, OPCPA) and difference frequency generation (DFG) setups. A compact and cost efficient octave-spanning MIR supercontinuum generator based on Cr:ZnSe has been reported in [121].

Second-order nonlinear susceptibility of ZnS and ZnSe ($d_{36} \approx 4$ and 16–20 pm/V, respectively) [127], [128] is comparable or higher than that of $LiNbO_3$. Polycrystalline ZnS and ZnSe consist of a multitude of microscopic single-crystal grains. The broad distribution of grain sizes and orientations allows for three-wave mixing via random quasi-phase-matching process (RQPM). The main distinctive features of RQPM (a linear dependence of the conversion yield with the medium length and an ultra-wide bandwidth) were predicted in [129], [130] and then confirmed in a proof-of-principle experiment [131]. RQPM is less efficient than the conventional QPM process in cw and ns pulsed laser regimes. However, a number of recent reports have demonstrated that RQPM in polycrystalline ZnS and ZnSe is very well suited for three-wave-mixing of few-cycle MIR pulses with high peak power and broad spectrum [132], [133].

Ultrafast sources based on Cr:ZnS and Cr:ZnSe can be used as laser frequency comb generators in the spectral range 2–3 μm with a number of important applications in science and technology [134]. Furthermore, Cr^{2+}-based sources provide a very convenient starting point for the extension of frequency combs to the whole MIR range of 2–20 μm. The standard approach to MIR comb generation is based on an intrapulse difference frequency generation (DFG) of ultra-short (sub-two-cycle) pulses from available fs lasers [135]–[138]. Advantages of this approach include inherent stability of carrier-envelope-phase and possibility to access the long-wavelength part of the MIR range (10–20 μm). The limitations of this approach arise from the intrinsic difficulty of simultaneously achieving high efficiency of the DFG process and a broad bandwidth of phase-matching.

Another approach to generation of MIR combs is presented by degenerate (subharmonic) parametric oscillators (OPO) [139]. Synchronous pumping of a subharmonic OPO by a frequency comb (fs pump laser) simultaneously provides frequency-divided-by-2 down-conversion and significant spectral broadening. Furthermore, the technique features high pump conversion efficiency and fully preserves the coherence of the pump comb [140].

The use of mode-locked Cr^{2+}-based lasers for OPO pumping has attracted a lot of attention. Subharmonic OPO and dual comb spectroscopy with fs Cr:ZnSe lasers were demonstrated shortly after the advent of first SESAM mode-locked oscillators [141], [142]. More recent achievements include a subharmonic OPO with instantaneous spectral span of 2.9–8.4 μm [143]. The most well-studied nonlinear material for Cr^{2+}-laser pumped OPOs is quasi-phase-matched orientation patterned GaAs (OP-GaAs) [143], [144]. A new route for generation of few-cycle pulses and multi-octave frequency combs has been opened by the world's first OPO based on RQPM in polycrystalline material (1.5-mm thick ZnSe sample) [145]. A number of similar polycrystals (ZnSe, ZnS, ZnTe, ZnO, CdSe, GaP, GaN) are readily available for OPO applications. Further in this section, we will demonstrate that the necessity to achieve phase-matching condition can be further relaxed in self-phase-matched OPOs based on sufficiently thin (of the order of coherence length) samples of nonlinear material.

With a few exceptions, the experiments were carried out in a standard lab environment at 40–60% relative air humidity.

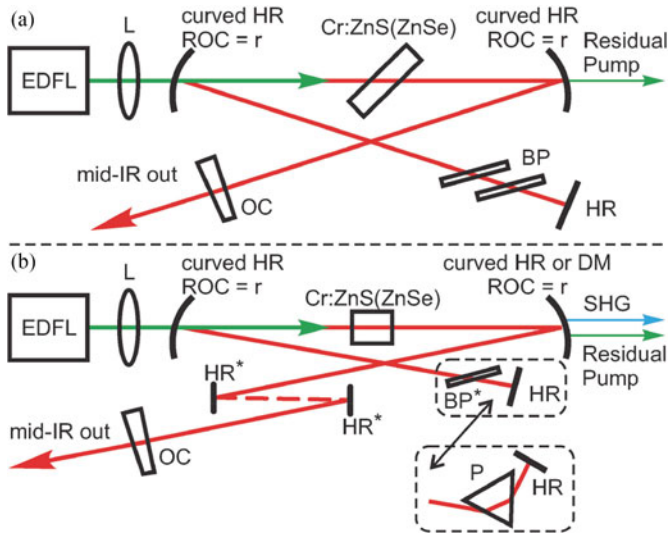

Fig. 19. Generic resonators of Kerr-lens mode-locked Cr:ZnS (ZnSe) oscillators (not to scale): (a) 1st generation lasers, (b) 2nd generation lasers. EDFL, pump laser at 1550–1567 nm; L, pump focusing lens; Cr:ZnS(ZnSe), gain element; HR, high reflectors; OC, output coupler; HR∗, optional folding high reflectors; BP, Brewster plates for dispersion control (YAG, FS, sapphire, etc.); BP∗ optional Brewster plate with low GDD and TOD for polarization control. SHG signal is generated in the gain element via RQPM process and separated by an optional dichroic mirror DM. Dashed rectangle shows an optional wavelength tuning stage that includes a CaF_2 prism (P) and a tuning HR, see main text.

Some MIR sources with ultra-broad spectra were purged by nitrogen, which will be specified in the main text. All obtained laser parameters correspond to long-term-stable laser operation in Kerr-lens mode-locked regime at fundamental repetition rate with linear polarization. Laser spectra were characterized using a Princeton Instruments SP2150 monochromator (150 and 75 g/mm gratings), InGaAs (Thorlabs), PbSe (Thorlabs), MCT (VIGO, Teledyne Judson) detectors and, if necessary, sets of spectral filters (Spectrogon). We did not post-process the acquired spectra to account for spectral dependences of the diffraction efficiency of the gratings and sensitivity of the detectors. Temporal parameters of the lasers were evaluated using an interferometric autocorrelator (A·P·E GmbH) with measurable MIR pulse widths of ∼20 fs. We relied on the autocorrelator's control software and used sech^2 fit of the autocorrelation functions for evaluations of the pulse duration. Output beam profiles were characterized by a bolometric camera (DataRay WinCamD-FIR2-16-HR). Femtosecond pulse trains at fundamental MIR wavelength and at second harmonic wavelength were detected by fast MCT and InGaAs photo detectors (VIGO PEM and Time-Base PD1800, respectively) and acquired by TDS7254 digital scope.

B. Kerr-Lens Mode-Locked Oscillators Based on Polycrystalline Cr:ZnS and Cr:ZnSe

The first Kerr-lens mode-locked Cr:ZnS and Cr:ZnSe lasers were very similar to well-established Ti:sapphire oscillators. A schematic of the 1st generation of Cr:ZnS(ZnSe) oscillators is illustrated in Fig. 19(a). These lasers rely on Brewster mounting of uncoated gain elements in the standard astigmatism compensated Z- or X- folded resonators. Another distinctive feature of this design is the use of plane-parallel Brewster plates as a primary means for dispersion control. Some IR materials (e.g., sapphire, YAG) have negative group delay dispersion (GDD) and hence can compensate for positive GDD of ZnS and ZnSe. On the other hand, the properties of optical materials in the range 2–3 μm are such that prism compensators do not bring much advantage in comparison with the plate compensators see, e.g., [108], [112].

The typical 1st generation laser setups are described in [73], [114]–[116]. These designs have allowed the attainment of ∼70 fs pulses with up to 6 nJ pulse energy and ∼75 kW peak power. The limitations of 1st generation lasers arise from thermal optical effects in the Brewster mounted gain elements (limitations on power) and from significant third-order dispersion (TOD), which is introduced by the plate compensator (limitations on pulse duration).

New and improved designs of Kerr-lens mode-locked Cr:ZnS and Cr:ZnSe lasers enabled significantly shorter pulses with higher average and peak power. Distinctive features of these 2nd generation lasers include (i) unconventional normal incidence mounting of the AR coated gain element and (ii) extensive use of the optical coatings with tailored chromatic dispersion. New laser designs were introduced in [28] and further developed in [117]–[119], [132]. Features of the 1st and 2nd generations were combined in a recent report on a Kerr-lens mode-locked polycrystalline Cr:ZnSe laser with conventional Brewster mounting of the gain element (and hence limited power) but advanced GDD and TOD control (and hence relatively short pulses) [146].

A generic scheme of a 2nd generation oscillator is shown in Fig. 19(b). The polycrystalline Cr:ZnS (Cr:ZnSe) gain element is 4–9 mm long, is optically pumped by off-the-shelf EDFL, and is cooled with RT water. The gain element is plane-parallel cut and AR coated. Typical low-signal transmission of the gain elements at the pump wavelength is 5–20%. The resonator includes two curved high reflectors (HR) with radii of curvature r, a plane end mirror and an output coupler for fundamental MIR radiation (OC). The choice of the radii of curved mirrors depends on the desired output parameters of the oscillator. The radii may vary from 150 mm [132] to 15 mm [119]. The resonator's legs are unequal with a typical ratio of 2:5 with the OC being installed in the longer leg. Optional folding mirrors HR∗ can be introduced in the resonator in order to reduce its foot-print. An optional output for second harmonic radiation can be implemented via curved dichroic mirror (DM) with high transmission in SHG range, as shown in Fig. 19(b). All optical coatings are dispersion-controlled. Currently we control net-GDD and TOD of the resonator within a third of an octave.

The angle of incidence at the curved mirrors is minimized to reduce the astigmatism of the resonator. Our experiments show that the residual astigmatism of the resonator is not an impediment for Kerr-lens mode-locking of Cr:ZnS and Cr:ZnSe lasers see, e.g., [119]. Circular or close-to-circular output beam profiles can be obtained in most cases.

Unconventional normal incidence mounting of the gain element provides (i) better management of the thermal optical effects due to circularity of the pump and laser beams, (ii) a

significant increase of the pump and laser intensity inside the gain element, (iii) greater convenience when using gain elements with a large length and, hence, high pump absorption.

Furthermore, the resonator does not include polarizing components. The degeneracy of two orthogonal polarizations is lifted only by the residual astigmatism of the resonator. Therefore, the output of a Kerr-lens mode-locked laser can be either p- or s- polarized, depending on the laser alignment. The laser design also allows simultaneous generation of two orthogonally polarized pulse trains at the fundamental repetition rate. If desired, an optional Brewster plate with low GDD and TOD can be introduced into the resonator for convenient polarization control.

We usually operate the oscillators near the maximum of the tuning curves at central wavelength $\lambda_C = 2.3$–2.4 μm. We use birefringent plates (see, e.g., [28]), or prisms (this paper) for wavelength tuning of the fs oscillators.

We first optimize the lasers for maximum cw output power. The distance between the curved mirrors is then fine-adjusted in order to enable Kerr-lens mode-locking (initiated by OC translation). A minimum pump power, which is necessary for achieving mode-locking, depends on the OC reflectivity and, to a lesser extent, on net-GDD of the resonator. The minimum pump power can be as low as 0.5 W at $R_{\rm OC} = 99\%$ and as high as 6 W at $R_{\rm OC} = 50\%$. An increase of pump power above the minimum by a factor of 1.5–2 usually results in multi-pulsing and in appearance of cw component in the emission spectrum.

Optimizations of the Kerr-lens mode-locked lasers for short pulse duration and for high output power include (i) fine-tuning of the resonator's net-GDD and compensation of TOD, (ii) optimization of OC's reflectivity $(R_{\rm OC})$, (iii) fine-tuning of pump power and pump focusing in the gain element, as described in [117].

The design of 2nd generation oscillators is very flexible, as illustrated in Fig. 20. We obtained few-cycle pulses with Watt-level average power at fundamental repetition rates (f) ranging from 70 MHz to 1 GHz. Output pulses as short as three (and, most likely, even two) optical cycles were achieved at repetition rates f $<$ 300 MHz. We believe that fine-tuning of the resonators will enable these short pulses at GHz repetition rates as well. Furthermore, high nonlinear indices and high laser gain in Cr:ZnS and Cr:ZnSe allows us to use output couplers with very high transmission $(R_{\rm OC} = 40 - 60\%)$, which is favorable for generation of few-cycle pulses with high energy (up to 24 nJ) and peak power (up to 1 MW).

Parameters of several selected laser configurations are summarized in Table V. To the best of our knowledge, these sets of parameters are record-high for fs MIR oscillators in the spectral range 2–3 μm. However, it is important to mention recent developments of Kerr-lens mode locked Ho:YAG thin-disk oscillators at 2 μm, which represent a new route for generation of fs pulses in the MIR [147], [148].

As can be seen from the table, polycrystalline Cr:ZnS and Cr:ZnSe enable unusual regimes of fs oscillators. For instance, achieved levels of peak power inside the resonator may exceed the critical power for self-focusing in the gain medium (lines 1, 4). On the other hand, RQPM in the gain medium results in SHG signals with sub-Watt power (line 1).

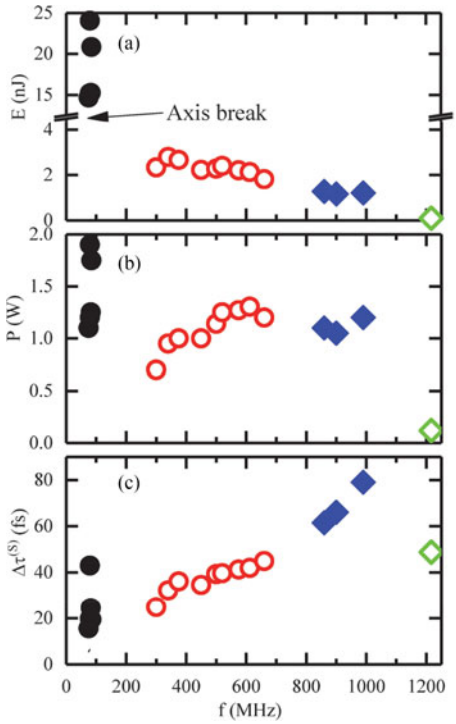

Fig. 20. Pulse energy E (a), average power P (b), pulse duration $\Delta\tau^{(S)}$ (c) of Kerr-lens mode-locked lasers vs repetition rate f. Pulse durations were derived from measured spectra of pulses assuming the time-bandwidth product 0.32. We used curved mirrors with different radii (r) and output couplers with different transmissions $(R_{\rm OC})$, including: • r = 100 mm, $R_{\rm OC} = 40$–90%; ◯ r = 50 mm, $R_{\rm OC} = 90\%$;◇ r = 30 mm, $R_{\rm OC} = 90\%$; ◇ r = 15 mm, $R_{\rm OC} = 99\%$.

Effects of high peak power on output pulses of fs Cr:ZnS laser are illustrated in Fig. 21. The design of the oscillator is described in [121]. Spectra of pulses significantly depend on the reflectivity of the output coupler $R_{\rm OC}$. Smooth spectra with 16.1 THz FWHM bandwidth (dashed curve in Fig. 21(a)) were obtained with $R_{\rm OC} = 40\%$ at 21 nJ output pulse energy. This corresponds to 1.5 MW intracavity peak power assuming time-bandwidth product of 0.32. Thus, the ratio of peak power to the critical power is $\kappa = P_{\rm Pk}/P_{\rm Crit} \approx 3.75$.

Installation of the OC with $R_{\rm OC} = 90\%$ has decreased output pulse energy to 6.3 nJ but provided approximately twofold increase of the parameter κ. Increased intracavity peak power resulted in strong broadening of pulses' spectrum to 31 THz FWHM. Significant optical signal at 2.6–2.8 μm suggests that an even broader spectrum can be obtained by purging the optical resonator.

Obtained spectra correspond to two-optical-cycle pulses $(\Delta\tau^{(S)} = 10 - 20$ fs, assuming time bandwidth product 0.32). These short pulses experience significant temporal broadening during propagation through the output couplers. 3.2 mm thick YAG $(R_{\rm OC} = 40\%)$ and ZnSe $(R_{\rm OC} = 90\%)$ substrates introduce GDD of -400 fs^2 and $+700$ fs^2, respectively, which results in temporal broadening of output pulses by 300–600%.

TABLE V
PARAMETERS OF KERR-LENS MODE-LOCKED POLYCRYSTALLINE CR:ZNS, CR:ZNSE LASERS[a]

#	P, W			f, MHz	$\Delta\tau$, fs	E, nJ	P_{Pk}, kW	R_{OC}, %	Medium	Ref
	Pump	MIR	SHG							
1	5.5	1.1	0.35[b]	75	15$^{(S)}$	14	900$^{(S)}$	60	Cr:ZnS	[121]
2	8.5	1.9	0.15	79	41	24	500	50	Cr:ZnS	[118]
3	2.0	0.25	0.04	83	43	3	60	90	Cr:ZnSe	[132]
4	9.5	1.8	~0.05	84	19$^{(S)}$	21	1000$^{(S)}$	40	Cr:ZnS	[119]
5	10	2.0	0.01	95	67	21	275	50	Cr:ZnS	[28]
6	5.9	0.8	~0.01	1060	125	0.75	5.3	90	Cr:ZnS	[121]
7	3.4	0.12	~0.01	1217	50	0.1	1.7	99	Cr:ZnS	[119]

[a]P, average power (Pump, MIR, and SHG wavelengths); E, pulse energy; $\Delta\tau$ pulse duration; P_{Pk}, peak power; R_{OC}, output coupler reflectivity (all for MIR band). $^{(S)}$ Estimated from measured spectra of pulses, assuming the time-bandwidth product 0.32.
[b]0.46 W SHG power inside the gain element.

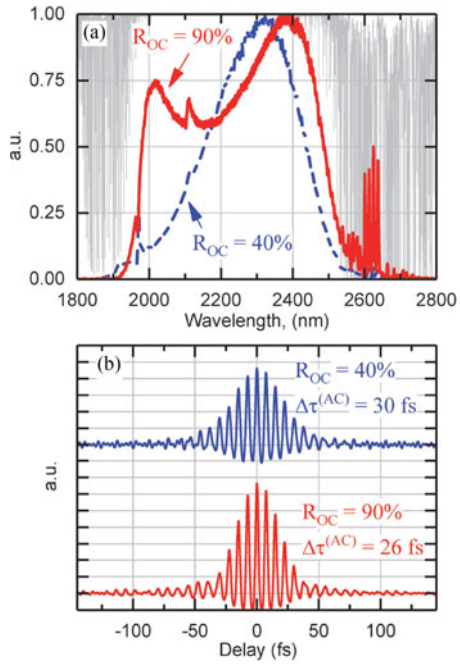

Fig. 21. Part (a) Spectra of pulses of Cr:ZnS oscillator at repetition rate f = 84 MHz. Two different output couplers (R_{OC} = 40% and 90%) provide different output pulse energies (21 nJ and 6.3 nJ, respectively) and different intracavity peak power (approximately 1.5 MW and 3 MW). Gray background in top graph shows transmission of 1 m standard air. Part (b) autocorrelations of output pulses. Pulses were re-compressed outside the resonator to compensate for OC's substrate dispersion (see main text). Pulse durations ($\Delta\tau^{(AC)}$) were estimated using sech^2 fit.

We re-compressed output pulses outside the resonator using the plane-parallel plates, as described in [121]. Autocorrelations of re-compressed pulses are illustrated in Fig. 21(b). The use of simple plate compressors allows for GDD compensation but retains significant uncompensated third order dispersion (TOD = +3000 fs^3). Therefore, output pulses have residual temporal broadening to 26–30 fs. Most likely, the use of mirror-based output compressors with GDD and TOD control will reveal sub-two-cycle MIR pulses.

An important feature of polycrystalline Cr:ZnS and Cr:ZnSe laser materials is RQPM, which enables three-wave mixing of few-optical-cycle pulses directly in the gain medium of a mode-locked laser. The fabrication of polycrystalline Cr:ZnS and Cr:ZnSe gain elements by post-growth thermal diffusion doping allows control of the microstructure of the material and hence tailoring of its parameters in favor of a certain type of three-wave mixing, e.g., SHG [121].

We evaluated the intracavity SHG in polycrystalline Cr:ZnS and Cr:ZnSe using gain elements with similar laser parameters but with significantly different microstructures. Two laser setups utilized the same EDFL pump, optical components, and dispersion compensation scheme. Two polycrystalline Cr:ZnS (Cr:ZnSe) gain elements were 5 mm (6 mm) long with 11% (12%) low-signal pump transmission. Two Kerr-lens mode-locked lasers were arranged to produce similar output pulses and fundamental wavelength, as described in [132], [133].

The theoretical treatment of RQPM in polycrystals predicts a loose dependence of the yield of three-wave mixing on the average size of the grains. The highest yield is reached if the average grain size equals the coherence length (l_C) of desired three-wave mixing [131]. The average size of the grain was about 30 μm for Cr:ZnS and about 500 μm for Cr:ZnSe. Thus, the Cr:ZnS gain element was optimized for efficient 2400 nm $\rightarrow$ 1200 nm SHG ($l_C \approx 30$ μm), while the Cr:ZnSe gain element was strongly mismatched with respect to the SHG process ($l_C \approx 20$ μm).

Parameters of two Kerr-lens mode-locked lasers are compared in Fig. 22. In both cases we obtained transform-limited 5-optical-cycle pulses at fundamental wavelength (λ_C = 2325 and 2420 nm for Cr:ZnS and Cr:ZnSe, respectively). In spite of higher nonlinearity, polycrystalline Cr:ZnSe exhibited relatively low SHG output: 40 mW vs 200 mW. This can be explained by a large mismatch of the grain size in the Cr:ZnSe sample, in full agreement with theoretical predictions. Spectra of SHG pulses as broad as 9.2 THz and 15 THz were obtained from Cr:ZnS and Cr:ZnSe, respectively. This exceeds the spectral width of pulses at fundamental wavelength (7.5 THz) and hence confirms ultra-broad bandwidth of RQPM process.

Thus, intracavity SHG in ultrafast polycrystalline Cr:ZnS and Cr:ZnSe lasers at 2–3 μm provides simple access to fs pulses in the range 1–1.5 μm with sub-Watt average power levels. Other sum-frequency mixings in polycrystalline Cr:ZnS and Cr:ZnSe [117], [133] provide opportunities for control and stabilization of generated MIR optical frequency combs.

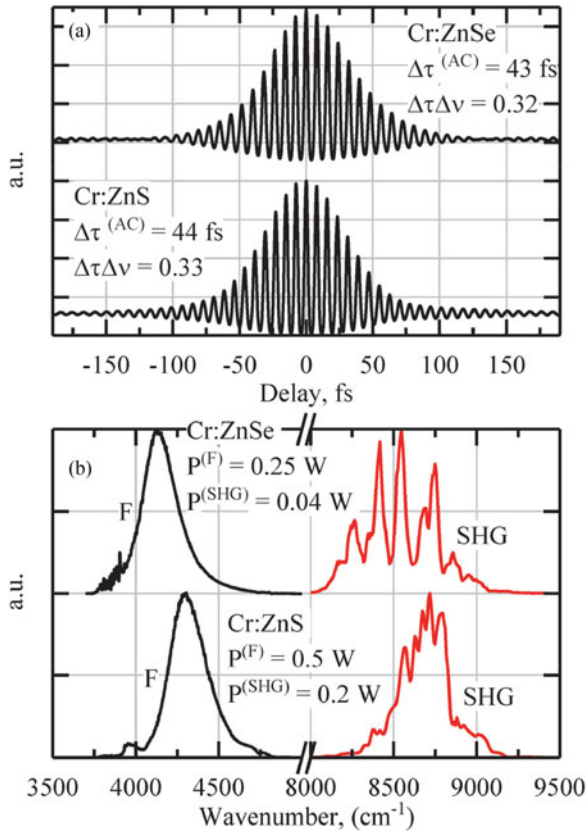

Fig. 22. Autocorrelations (a) and spectra of pulses (b) of Kerr-lens mode-locked polycrystalline Cr:ZnS and Cr:ZnSe lasers. Two lasers have very similar resonators at repetition rate f ≈ 80 MHz, with net-GDD of about -1500 fs^2, $R_{OC} = 10\%$. Autocorrelations were measured at fundamental wavelength. Pulse durations $(\Delta\tau^{(AC)})$ were estimated using sech^2 fit. Spectra of pulses are shown at fundamental spectral band (F) and at second harmonic (SHG). SHG occurs directly in the polycrystalline gain elements due to RQPM process.

Furthermore, RQPM allows for down-conversion of fs pulses via DFG and optical parametric process [143].

An important advantage of Cr:ZnS and Cr:ZnSe laser materials is their broad MIR tunability. For instance, continuous tuning of a narrowband cw Cr:ZnS laser in the range 1.88–3.05 μm has been demonstrated (see Section III). In a proof-of-principle experiment we implemented (i) Kerr-lens mode-locking of a Cr:ZnS laser at non-standard central wavelength and (ii) tuned the mode-locked laser around this wavelength.

The setup was similar to that shown in Fig. 19(b). The laser was equipped with 5 mm long polycrystalline Cr:ZnS gain element (11% low-signal pump transmission). The oscillator's repetition rate was set to f = 82 MHz. We used an output coupler with $R_{OC} = 60\%$ and dispersive mirrors, which were optimized for the central wavelength of 2200 nm. Net-GDD of the resonator was set to about -200 fs^2 within a third of an octave. The Kerr-lens mode-locked laser was first optimized for shortest pulse duration in a nonselective resonator. The obtained spectrum of the oscillator at 1.2 W power is shown in Fig. 23(a) and corresponds to $\Delta\tau^{(S)} = 25$ fs pulses assuming time bandwidth product is 0.32. We then equipped the resonator with a wavelength tuning stage. The stage consists of a CaF_2 prism (apex angle 70°) and a tuning HR mirror, as shown in Fig. 19(b).

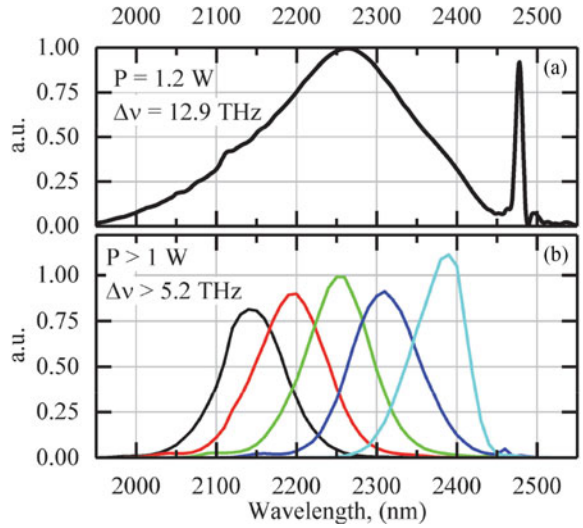

Fig. 23. Spectra of pulses of Cr:ZnS oscillator at repetition rate f = 82 MHz. Dielectric coatings were optimized for fs laser operation at central wavelength 2200 nm (see main text). Part (a) Nonselective resonator. Part (b) the resonator is equipped with the wavelength tuning stage. The spectrum at 2250 nm central wavelength is normalized to unity and other spectra are normalized to power.

We obtained a continuous tuning of the mode-locked laser in the range 2100–2400 nm with an average power in excess of 1 W and pulse duration $\Delta\tau^{(S)} = 50 - 60$ fs.

As can be seen, the very simple single-prism design of the tuning stage provides broad tuning range and relatively short, 6–8 optical cycles, output pulses. This can be explained by low chromatic dispersion and low group velocity dispersion of CaF_2 (and other fluorides, e.g., BaF_2) in the range 2–3 μm. So the use of a fluoride prism provides just sufficient selectivity for central wavelength tuning but results in relatively small reduction of the spectral bandwidth of pulses.

Thus, the results presented in this section demonstrate that Kerr-lens mode locked lasers based on polycrystalline Cr:ZnS and Cr:ZnSe have come of age and, arguably, represent the most viable route for generation of ultra-short pulses in the range 2–3 μm. Developed designs of Kerr-lens mode locked oscillators feature high efficiency and provide access to few-cycle MIR pulses with Watt-level power in a very broad range of pulse repetition rates.

C. Power and Energy Scaling of Femtosecond Middle IR Pulses in Single-Pass Cr:ZnS and Cr:ZnSe Amplifiers

Cr:ZnS and Cr:ZnSe provide many possibilities for power and energy scaling of fs pulses. The materials fully support all standard techniques of chirped pulse amplification (CPA). For instance, a compact kHz CPA with 1 mJ pulses and 5 GW peak power has been reported [109]. Additionally, the relatively high cross sections and long lifetimes of these materials (see Table IV) enable extremely compact and robust single-pass amplifiers with unique combinations of output parameters.

The advantages of a single-pass Cr:ZnS amplifier in fs laser regime were first evaluated in [116]. The single-pass designs were further improved in [120], [121], [149]. The schematic of a single-pass Cr:ZnS (Cr:ZnSe) amplifier is illustrated in Fig. 24.

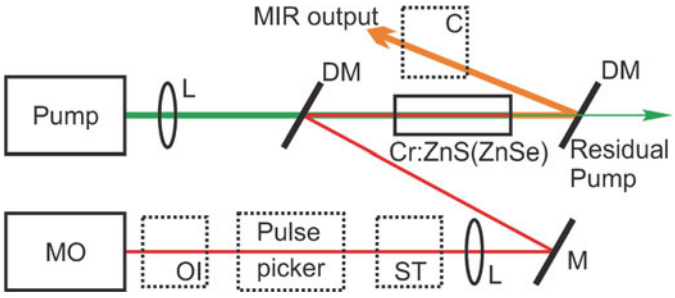

Fig. 24. Generic single-pass ultrafast amplifier (not to scale): (Cr:ZnS/ZnSe), amplifier's gain element; (Pump), cw or pulsed laser for optical pumping; (MO), fs master oscillator; (L), lenses for focusing and mode-matching of Pump and MO beams; (M) beam steering mirrors; (DM), dichroic mirrors for combining and separation of Pump and MO radiations. Dotted rectangles show optional components, including: (OI), optical isolator; pulse picker; (ST), pulse stretcher; (C), pulse compressor.

The amplifier is seeded at 2–3 μm by a fs MO. The amplifier is optically pumped at 1.5–2 μm by cw or pulsed laser, e.g., Er- or Tm- doped fiber laser, Er:YAG laser, Ho:YAG laser, etc.

Single-pass arrangement of the amplifier provides robustness and, at the same time, great flexibility. The system can be configured for a number of distinctly different regimes, depending on a combination of three parameters f, γ, κ.

- f The amplifier can be either operated at full repetition rate of the master laser or include a pulse picker. Thus the parameter f can be chosen in a range from 10^0 to 10^9 Hz.
- γ Depending on a ratio of pump power to average power of the seed ($\gamma = P_{\mathrm{Pump}}/P_{\mathrm{Seed}}$) or a ratio of pump pulse energy to pulse energy of the seed ($\gamma = E_{\mathrm{Pump}}/E_{\mathrm{Seed}}$), the amplifier can be either configured for high gain or for high pump conversion with moderate gain. The parameter γ can be chosen in a range from 10^0 to 10^6.
- κ Nonlinear interactions in the amplifier can be described by a ratio of peak power of pulses, which is achieved inside the gain element, to the critical power for self-focusing in the medium ($\kappa = P_{\mathrm{Pk}}/P_{\mathrm{Crit}}$). This parameter can also be controlled in a broad range from 10^{-2} to 10^2.

We implemented four configurations of Cr:ZnS and Cr:ZnSe single-pass amplifiers with the following combinations of the parameters:

a) f = 0.9 GHz, $\gamma = 18$, $\kappa \approx 10^{-1}$, $\Delta\tau = 80$ fs (i.e., very high pulse repetition rate, high efficiency, low nonlinearity, ten-cycle seed pulses);
b) f = 81 MHz, $\gamma = 13$, $\kappa \approx 10^0$, $\Delta\tau = 50$ fs (high repetition rate, high efficiency, significant nonlinearity, six-cycle seed pulses);
c) f = 76 MHz, $\gamma = 17$, $\kappa \approx 10^0$, $\Delta\tau \approx 20$ fs (high repetition rate, high efficiency, significant nonlinearity, very short 2.5-cycle seed pulses).
d) f = 1 kHz, $\gamma = 5{\cdot}10^5$, $\kappa \approx 10^2$, $\Delta\tau \approx 20$ fs (low rate, very high gain, very high nonlinearity, very short 2.5-cycle seed pulses).

The laser setups (a) and (b) are described in detail in [119], [120], [121]. Single pass amplifiers were operated at full repetition rate of the maser lasers and were continuously pumped at 1567 nm by off-the-shelf EDFLs with 20 W power.

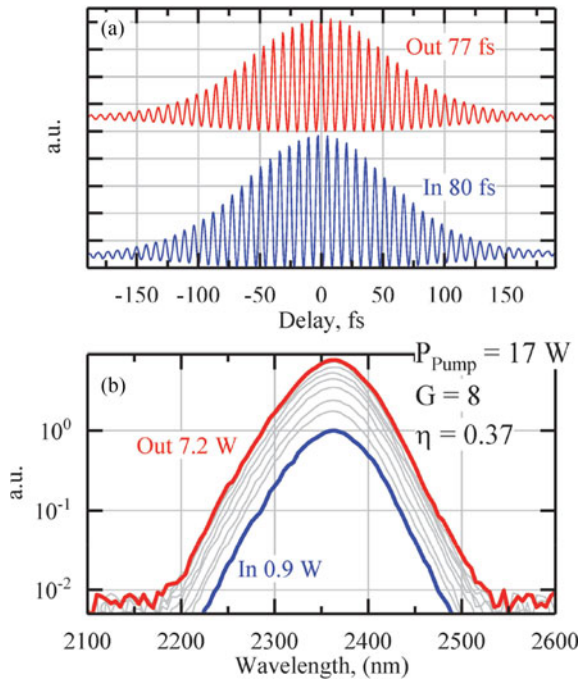

Fig. 25. Measured autocorrelations (ACs, a) and spectra of pulses (b) of Cr:ZnS amplifier at f = 0.9 GHz. Initial AC (In, amplifier's pump is off) is compared with the final AC (Out, full pump power). Numbers near ACs show estimated pulse durations (sech^2 fit). Initial spectrum (In, blue) normalized to unity; final spectrum (Out, red) normalized to optical power; grey lines show intermediate spectra, obtained during the gradual increase of pump power (normalized to power). Numbers near the spectra show output power (P) measured without pumping (In) and at full pump power (Out).

Chromatic dispersion of the 9 mm long AR coated polycrystalline Cr:ZnS gain elements of the amplifiers was compensated by a combination of dispersive mirrors.

Parameters of the single-pass amplifier in configuration (a) are summarized in Fig. 25. As can be seen, the amplifier fully preserves spectral and temporal parameters of seed pulses. We measured MIR output power in excess of 7 W at 17 W power of EDFL pump. This corresponds to 100 kW peak power of output pulses and rather high ($\eta = 37\%$) conversion efficiency of cw EDFL radiation to fs MIR pulses. To the best of our knowledge, this is the highest power from a MIR fs source at GHz repetition rate. Furthermore, because of a high fundamental repetition rate, the footprint of the whole master oscillator single-pass amplifier setup was as small as 20×20 cm^2 (excluding EDFLs). We used the standard optical mounts and did not put any special effort into the footprint reduction. Therefore, significantly more compact MIR fs source at a GHz repetition rate can be implemented.

Configuration (b) of the single-pass amplifier was seeded at lower rate (81 MHz) by shorter pulses (50 fs) with significantly higher initial peak power 350 kW (i.e., at the initial $\kappa \approx 1$). Our experiments show that an interplay between laser and nonlinear interactions inside the amplifier's gain medium results in simultaneous amplification and spectral broadening of seed pulses. The spectral broadening exhibits a threshold-like behavior. The broadening becomes significant if the parameter κ inside the amplifier's gain medium approaches $\kappa \approx 3$ (1.2–1.5 MW peak power of pulses in Cr:ZnS) [121]. Parameters of the single-pass

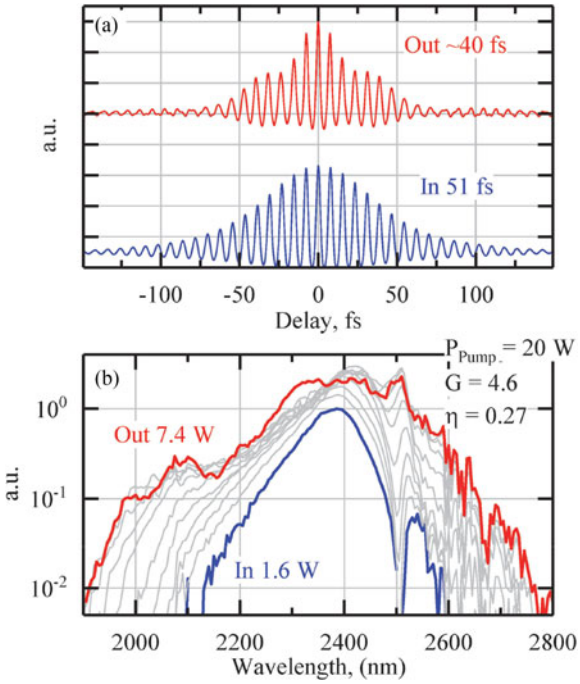

Fig. 26. Measured autocorrelations (ACs, a) and spectra of pulses (b) of Cr:ZnS amplifier at f = 81 MHz. Initial AC (In) is compared with the final AC (Out). Numbers near ACs show estimated pulse widths ($sech^2$ fit). Initial spectrum (In, blue) normalized to unity; final spectrum (Out, red) normalized to optical power; grey lines show intermediate spectra, obtained during the gradual increase of pump power (normalized to power). Numbers near the spectra show output power (P) measured without pumping (In) and at full pump power (Out).

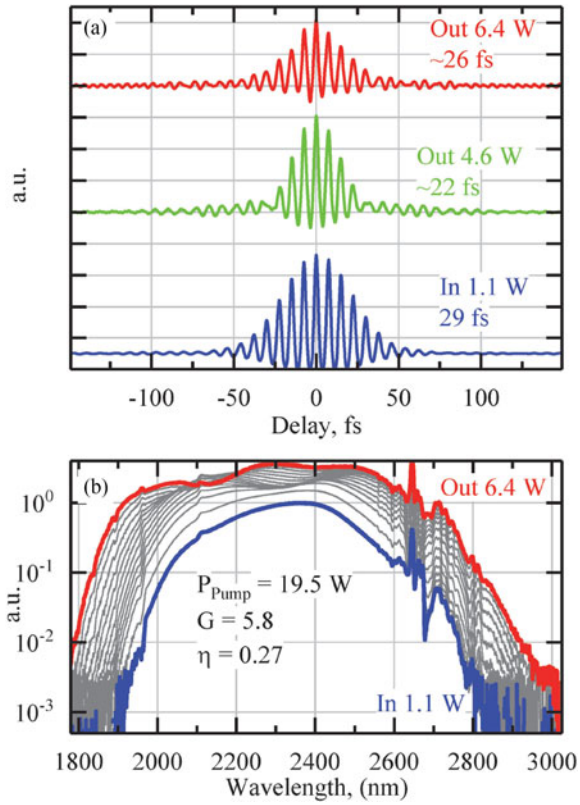

Fig. 27. Measured autocorrelations (ACs, a) and spectra of pulses (b) of Cr:ZnS amplifier at f = 76 MHz. Initial AC (In) is compared with ACs of amplified pulses at 4.6 W and 6.4 W output power. Numbers near ACs show estimated pulse widths. Initial spectrum (In, blue) normalized to unity; final spectrum (Out, red) normalized to optical power; grey lines show intermediate spectra, obtained during the gradual increase of pump power (normalized to power). Numbers near the spectra show output power (P) measured without pumping (In) and at full pump power (Out). The laser setup was purged by nitrogen. The path from the output window to the input slit of the monochromator (0.25 m) and the monochromator itself were unpurged with 40% relative air humidity.

amplifier in configuration (b) are summarized in Fig. 26. Part (b) of the figure illustrates variation of spectra of output pulses with increase of the amplifier's gain. Spectral broadening as high as 65% (at −20 dB level) was obtained at the maximum gain G = 4.6.

Fig. 26(a) shows autocorrelations of input and output pulses. As can be seen, amplified pulses were compressed by 20% to 5 optical cycles. Autocorrelation of output pulses reveals significant residual chirp. Most likely, better dispersion control of the amplifier will result in even shorter pulses: 13 THz (FWHM) broad output spectrum allows us to estimate pulse width of 30 fs assuming time-bandwidth product of, e.g., 0.4.

In the next experiment we evaluated the same single pass amplifier in the regime of two-optical-cycle seed pulses. The master oscillator has been optimized for 17.4 THz FWHM bandwidth ($\Delta\tau^{(S)} \approx 18$ fs) with 1.1 W average power and 700 kW peak power at 76 MHz repetition rate. We used the same combination of dispersive mirrors and an additional Brewster mounted plane-parallel YAG plate with 4 mm thickness for dispersion control. The setup was purged by nitrogen. We obtained 6.4 W output power at single-pass gain of G = 5.8 and 27% conversion efficiency. Spectra and autocorrelations of initial and amplified pulses are compared in Fig. 27. Spectral bandwidth of pulses has increased from 325 nm to 640 nm (FWHM) and from 950 nm to 1250 nm at −30 dB level. Autocorrelations of amplified pulses allow us to estimate 22 fs pulse width at 4.6 W output power and 26 fs pulse width at maximum 6.4 W output power. We expect that the use of advanced methods for the characterization of ultrashort pulses, e.g., frequency-resolved optical gating [150], and further improvements in the dispersion control will result in sub-two-cycle pulses.

In the subsequent experiment the single-pass amplifier was configured for even higher gain and nonlinearity (configuration (d) with f = 1 kHz, $\gamma = 5 \cdot 10^5, \kappa \approx 10^2$). Cw EDFL pump was replaced by a Q-switched Er:YAG laser at 1645 nm with 4 mJ pulse energy and 200 ns pulse width at 1 kHz repetition rate. The setup was equipped with a pulse picker (based on RTP Pockels cell, Raicol) and with an optical isolator (Thorlabs). We also replaced the output dichroic mirror (right DM in Fig. 24) with a gold-coated mirror. The amplifier was seeded with 15 nJ, 30 fs pulses at 2350 nm central wavelength.

As the amplifier's gain element we used a Brewster-cut 30 mm long Cr:ZnSe with high dopant concentration ($5 \cdot 10^{18}$ cm^{-3}), and with <0.01% initial transmission at pump wavelength. The average size of the grains in the polycrystalline gain element was as large as 500–1000 μm. Hence, SHG and sum frequency generation (SFG) due to RQPM in the gain medium were suppressed.

Seed pulses were stretched to about 300 fs during their propagation trough the master laser's OC, the optical isolator, and the

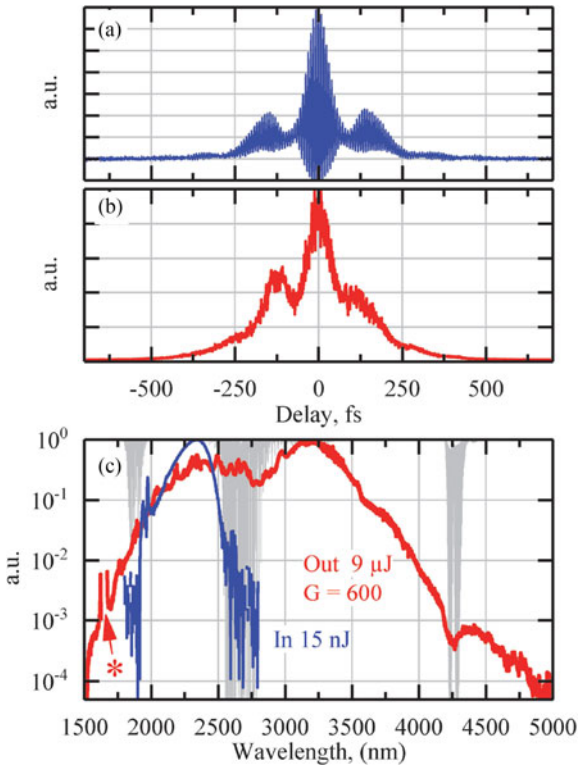

Fig. 28. Measured autocorrelations (ACs, a, b) and spectra (c) of pulses of Cr:ZnSe amplifier at f = 1 kHz. (a), interferometric AC of 'cold' amplifier was measured while the pump and the pulse picker were off. (b), Intensity AC of 'hot' amplifier at f = 1 kHz, 9 μJ output pulse energy. (c), spectra of seed (In) and amplified (Out) pulses are compared. We stitched together several spectra, which were measured with extended InGaAs and MCT detectors in combination with Ge and LP-3000 filters. Asterisk shows residual pump at 1645 nm. Gray background shows transmission of 1 m standard air.

pulse picker. The main contributor to the input pulse stretching was 20 mm long RTP cell with negative GDD of -5000 fs^2. On the other hand, the 30 mm long Cr:ZnSe gain element has a large positive GDD ($+7000$ fs^2). Therefore, seed pulses were simultaneously amplified and compressed during their propagation through the gain element.

Results of the experiment are summarized in Fig. 28. Top autocorrelation was acquired by an interferometric autocorrelator at full repetition rate of the master laser (79 MHz) while both the amplifier's pump and the pulse picker were off (cold amplifier). As can be seen, output pulses of the cold amplifier are chirped. This can be explained by significant residual GDD and TOD of the setup ($+2000$ fs^2 and $+28000$ fs^3, respectively).

We then engaged the pulse picker and increased energy of pump pulses to 4 mJ. Autocorrelation and spectrum of amplified pulses at a repetition rate of f = 1 kHz are shown in parts (b) and (c) of the figure, respectively. The amplifier's gain was evaluated using a DC coupled photoelectromagnetic MIR detector with ns resolution, as described in [121]. We obtained single-pass gain G = 600 at >20 dB contrast of main pulses at f = 1 kHz with respect to the background.

Amplification of seed pulses well above the critical power for self-focusing in ZnSe resulted in generation of an octave-spanning supercontinuum (SCG) directly in the gain element of a single-pass amplifier. Obtained spectrum of amplified pulses with 9 μJ energy is shown in Fig. 28(c) and compared with spectrum of initial 15 nJ pulses. We did not observe significant fluctuations or degradation of the spectrum during multi-hour experiments.

An important feature of femtosecond SCG in bulk dielectrics is the high temporal coherence of the SC radiation and great compressibility of output SC pulses [126]. Therefore obtained spectral span of 1.8–4 μm (at -20 dB level) suggests the possibility of re-compression of the amplifier's output to sub-two-cycle MIR pulses. Furthermore, high $\chi^{(2)}$ and RQPM in polycrystalline ZnSe provides significant optical signals at second and higher optical harmonics. An interplay between $\chi^{(2)}$ and $\chi^{(3)}$ interactions during SCG in ZnSe has been recently studied in [125].

To conclude this section, we have demonstrated that single-pass ultrafast amplifiers based on polycrystalline Cr:ZnS and Cr:ZnSe provide rich opportunities for power end energy scaling of few-cycle MIR pulses. Very simple, compact and robust full repetition rate single-pass amplifiers enable few-cycle MIR pulses with multi-MW peak power. The sources feature small footprints and high (27–37%) conversion of low-cost cw EDFL radiation to ultra-short MIR pulses. On the other hand, very high single-pass gain (up to 30 dB) can be achieved with pulse down-picking to kHz repetition rate and with pulsed optical pumping of the amplifier by a Q-switched laser. Furthermore, single-pass amplifiers provide the capability to control (and even improve) spectral and temporal parameters of amplified pulses. Obtained parameters of the amplifiers are summarized in Table VI. In our opinion, these sets of parameters are either record-high or compete with other MIR fs sources in terms of efficiency and compactness of the laser setups.

D. Nonlinear Conversion of fs Cr:ZnS and Cr:ZnSe Lasers in Synchronously Pumped Optical Parametric Oscillators

Ultrafast Cr:ZnS and Cr:ZnSe lasers in the range 2–3 μm enable MIR comb generators with exceptional output parameters. The use of Cr^{2+}-based sources for pumping of DFG and OPO setups provides a number of advantages: (i) low energy of MIR photons (0.5 eV) reduces probability of multi-photon absorption in nonlinear media, (ii) multi-MW peak power of few-cycle pulses is achieved at a relatively low pulse energy further reducing the probability of damage of nonlinear media; (iii) few-cycle Cr:ZnS and Cr:ZnSe lasers with multi-Watt power are available in a broad range of repetition rates, (iv) fs Cr:ZnS and Cr:ZnSe lasers are pumped by readily available cw EDFLs with 25–30% conversion efficiency. The combination of features (i) and (ii) is especially important as it enables high yield of DFG or high parametric gain in thin samples of nonlinear materials. Many applications also require (or would benefit from) comb generators with high average power.

A generic scheme of synchronously pumped MIR OPO is illustrated in Fig. 29. Detailed description of the experiment can be found in [143], [144]. The system consists of a cw EDFL pumped fs Cr:ZnS (or Cr:ZnSe) laser system and an OPO resonator. Spatial mode-matching of the fs laser beams is

TABLE VI
PARAMETERS OF SINGLE-PASS POLYCRYSTALLINE CR:ZNS, CR:ZNSE MIR FS LASER AMPLIFIERS[a]

#	f, MHz	$\Delta\tau$, fs	λ_C, nm	$\Delta\nu$, THz	E, nJ	P_{Pk}, MW	P, W	Gain	Medium	Ref
1	900	77	2360	4.1 (19.7)	8	0.1	7.2	8	Cr:ZnS	[119], [121]
2	81	40	2385	12.7 (54)	91	2	7.4	4.6	Cr:ZnS	[120], [121]
3	76	26	2325	22 (68)	84	2.9	6.4	5.8	Cr:ZnS	This paper
4	0.001	300$^{(Ch)}$	2910	41 (107)	9000	30$^{(Ch)}$	0.009	600	Cr:ZnSe	This paper

[a]f, pulse repetition frequency; $\Delta\tau$ pulse duration; λ_C, central wavelength; $\Delta\nu$ spectral bandwidth FWHM (−30 dB); E, pulse energy; P_{Pk}, peak power; P, average power. $^{(Ch)}$ Chirped output pulses without re-compression.

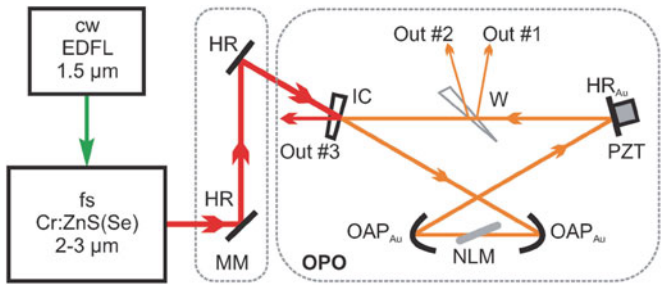

Fig. 29. Generic scheme of synchronously pumped OPO (not to scale): fs Cr:ZnS(Se) source at 2–3 μm is optically pumped by cw EDFL. Ring resonator of the OPO includes: gold coated plane and parabolic mirrors (HRAu, OAPAu) input coupler for pump laser radiation (IC), Brewster mounted plate made of nonlinear material (NLM). Length of the OPO resonator is controlled by a piezo transducer (PZT). A wedge (W) with small apex angle is used for dispersion control and outcoupling. A combination of mirrors (MM) is used for coupling of the fs pump beam in to the OPO resonator and for mode-matching.

implemented by a combination of plane and curved mirrors (MM). A bow-tie ring resonator of the OPO includes two off-axis gold-coated parabolic mirrors (OAP), a dielectric coated, dispersion controlled input coupler for pump pulses (IC) and a gold coated high reflector (HR). The system can be configured for a very broad range of repetition rates (0.08–1 GHz), which correspond to 3.75–0.3 m long OPO resonators. Additional folding HR mirrors are usually introduced in the ring resonator in order to reduce its footprint at low repetition rates. A thin wedge (W) with small apex angle is installed in the resonator between two plane mirrors. The wedge is used for dispersion control and as a broadband output coupler for signal/idler waves (outcoupling is adjusted by tilting the wedge near Brewster's angle). The OPO's engine is an uncoated plane-parallel polished plate made of nonlinear material (NLM), which is installed in the resonator at Brewster's angle between two parabolic mirrors.

The OPO oscillates only when the doubly-resonant condition is met, which corresponds to several discrete values of the cavity length separated (in terms of roundtrip) by approximately the pump wavelength (about 2.4 μm, in our case) [143], [144]. The number of resonances depends on pump power, losses in the OPO resonator, and chromatic dispersion of the nonlinear material. These resonance conditions are usually achieved by scanning the resonator's length by a piezo transducer attached to a mirror (PZT in Fig. 29). The standard techniques of servo control allow locking the OPO to a particular resonance [151].

We implemented two different OPOs using the ultrafast Cr:ZnS MOPAs (a) and (b), which were described in Section IV-C. The first OPO was based on conventional OP-GaAs material (0.5 mm thick, QPM period 88 μm, BAE Systems). The OPO was pumped by a 7 W MOPA at 0.9 GHz repetition rate. The OPO resonator was enclosed and purged by nitrogen, while the Cr:ZnS MOPA was operated in a standard lab environment. Parameters of the fs pump are summarized in Fig. 25. More details about the OPO setup can be found in [152].

High repetition rate of pump pulses has allowed us to reduce the footprint of the OPO resonator to 12 × 18 cm^2. On the other hand, pulses with 100 kW peak power were adequate for pumping of relatively narrow bandgap GaAs (2.35 μm central wavelength of pump pulses corresponds to three-photon regime of nonlinear absorption in GaAs).

Scanning of the OPO resonator's length by a piezo transducer (PZT) around synchronous pumping resonances is illustrated in Fig. 30(a). The OPO operates at six discrete lengths of the resonator. One of those peaks has the broadest instantaneous spectrum and corresponds to the degeneracy of the OPO, see, e.g., [143]. We measured the output spectrum while the OPO's resonator was dithered near its work point. The detected peak-shaped periodic signal was demodulated by a lock-in amplifier. The obtained spectrum is shown in Fig. 30(b) and is compared with a spectrum of pump pulses at 2.35 μm. Obtained spectral span was limited by the parameters of the input coupler and hence can be further improved.

The available pump power at 2.35 μm was sufficiently high to enable the thermal self-stabilization of the OPO resonator to the pump pulse train [153]. Measured average power of thermally-locked OPO was >0.2 W per each reflection from the outcoupling wedge (thin ZnSe with 1° apex angle, Outputs #1 and #2 in Fig. 29). Taking into account the losses on the LP3000 filter, which was installed before the power meter, one can estimate overall MIR power in excess of 0.5 W. To the best of our knowledge, we obtained by far (i) the highest power in this broad spectrum with (ii) the highest (2%) conversion efficiency of low-cost cw EDFL radiation, using (iii) the smallest footprint (only 0.06 m^2 was occupied by Cr:ZnS lasers and the OPO resonator). Relatively low pump depletion (about 40%) was measured at auxiliary Output #3. Therefore, the parameters of the OPO can be further improved.

In the next, proof-of-principle experiment we implemented an OPO based on a thin plate made of single-crystal ZnSe. The thickness of the plate (100 μm) was of the order of the coherence length of 2.4 μm → 4.8 μm frequency divide-by-two parametric process. Thus, the limitations on the phase-matching

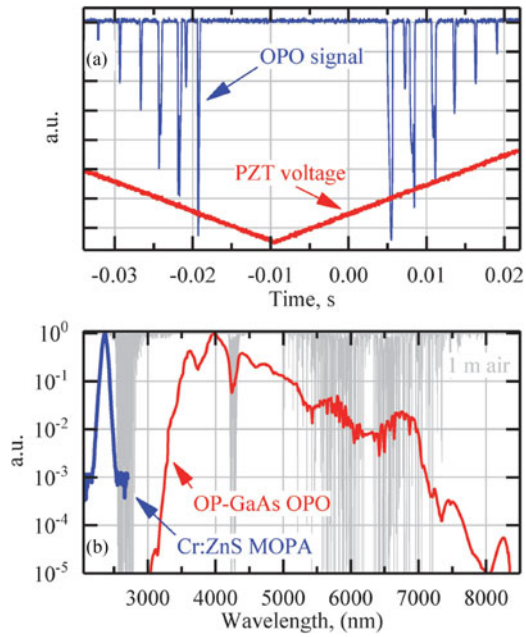

Fig. 30. Part (a) Detected OPO output (after LP-3000 filter) vs. time. The length of the OPO resonator is scanned at 10 Hz rate by a PZT. Consecutive peaks of OPO generation are separated by about 2.4 μm. Part (b) Measured spectrum of degenerate OPO (right) is compared with spectrum of pump pulses (left). Gray background shows transmission of 1 m standard air. We used Princeton SP2150 monochromator with 150 g·mm^{-1} grating and LN cooled MCT detector (Teledyne Judson). We stitched together several spectra, which were measured with LP3000, LP4500, and LP5000 filters (Spectrogon) and then normalized the resultant spectrum to unity. We did not post-process the spectrum to account for spectral dependences of the diffraction efficiency of the grating, sensitivity of the detector and filters' transmission.

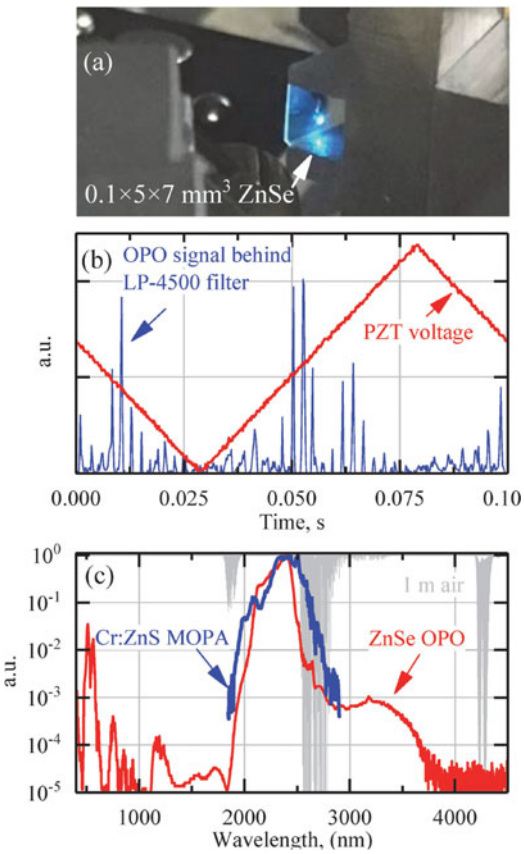

Fig. 31. Part (a) A photo of an OPO engine (100 μm thick plate made of single-crystal ZnSe installed in the OPO resonator). Blue emission in ZnSe is due to the multi-photon ionization followed by a recombination of free-carriers. Part (b) Detected OPO output (after LP-4500 filter) vs. time. The length of the OPO resonator is scanned at 10 Hz rate by a PZT. Part (c) Measured spectrum of the OPO is compared with spectrum of pump pulses. Gray background shows the transmission of 1 m standard air. Pump pulses are focused into a Ø10–15 μm spot resulting in intensity $>10^{12}$ W/cm^2.

bandwidth of the parametric interaction, which arise due to chromatic dispersion in the nonlinear material, were lifted.

The OPO was synchronously pumped by 7 W Cr:ZnS fs MOPA at 81 MHz repetition rate. Parameters of the pump source are summarized in Fig. 26. 5-optical-cycle pump pulses with up to 91 nJ pulse energy and 2 MW peak power were focused into a Ø10–15 μm spot. This provided pump intensity (I) and parametric gain (g) in the ZnSe sample in excess of 1 TW/cm^2 and 10 dB, respectively. Modification of the refractive index of ZnSe due to the Kerr effect was as high as $n_2 \cdot I \approx 0.02$ (1%). Wide 2.7 eV bandgap of ZnSe corresponds to five-photon regime of nonlinear absorption of pump pulses.

Results of the experiment are summarized in Fig. 31. Part (a) of the figure shows a photo of the ZnSe OPO engine in action. The intensity of pump pulses is sufficiently high to result in significant multi-photon ionization in ZnSe. Recombination of the free-carriers results in distinctive blue emission from ZnSe plate. Pumping of ZnSe at full 7.4 W pump power resulted in rapid degradation of the plate (apparently due to excessive multi-photon absorption and overheating of the pumped region). Therefore, the main experiments were carried out at reduced pump power (4.5 W).

We observed parametric oscillations in this synchronously pumped ZnSe OPO. However, the output parameters of the OPO were significantly different from those of the standard double resonant $\chi^{(2)}$ OPO, which operates close to the degeneracy (see, e.g., parameters of conventional OP-GaAs OPO in Fig. 30). Scanning of the OPO resonator's length around the synchronous pumping work-point provided an unusually large number OPO emission peaks in very broad range of the resonator's lengths. Pump depletion was very low (<5%). Furthermore, the OPO spectrum was truncated at about 3.5 μm. We used a combination of long-pass filters (Spectrogon LP-4500, LP-5000) to confirm the presence of the optical signal at the wavelengths above 5000 nm. However, the detected long-wave signal was too weak for spectroscopy and is not shown in Fig. 31(c).

We explain the peculiar behavior of this OPO by very high intensity of pump pulses (0.7 TW/cm^2). This creates high concentration of free carriers in ZnSe due to the multi-photon ionization. The free carriers induce strong MIR absorption with approximately λ^3 dependence on the wavelength [154]. Therefore, the conventional three-wave mixing regime of the parametric interaction is suppressed. Most likely, the OPO operates in a degenerate four-wave mixing regime, which arises from $\chi^{(3)}$ nonlinearity and is usually realized in fiber-based devices (see, e.g., [155]). Thus, achieved parameters of fs Cr^{2+}-based sources at 2–3 μm enable new self-phase-matched thin-plate OPOs. Essentially any nonlinear material (in the form of a sufficiently thin plate) is now available for fs OPO experiments.

Apparently, ZnSe is not best suited for thin-plate OPO applications and a search for an alternative material with better balance between the bandgap and the nonlinear susceptibilities is required in order to implement the OPO with competitive output characteristics.

E. Conclusion

Our review demonstrates that polycrystalline Cr:ZnS and Cr:ZnSe offer unique possibilities for the generation, amplification and nonlinear frequency conversion of ultra-short optical pulses in the MIR range. Cr^{2+}-based lasers now provide the shortest pulses (2–5 optical-cycles) with the highest average power (in excess of 7 W) with the broadest selection of repetition rates (0.07–1.2 GHz). The oscillators and amplifiers are conveniently pumped by off-the-shelf cw fiber lasers with high optical-to-optical conversion efficiency (20–40%).

Random quasi phase matching in polycrystalline Cr:ZnS and Cr:ZnSe is well suited for efficient three-wave mixing of few-optical-cycle pulses directly in the gain elements of ultrafast lasers and amplifiers. Significant optical signals at second, third and fourth optical harmonics can be used for control and stabilization of generated MIR optical frequency combs. Sum frequency mixing between MIR and pump radiations provides for referencing of generated MIR comb to the pump laser at 1.5–2 μm (e.g., stabilized cw or pulsed fiber laser). Furthermore, RQPM enables down-conversion of fs pulses to the MIR range of 3–10 μm. Fabrication of polycrystalline Cr:ZnS and Cr:ZnSe gain elements with tailored microstructure (to favor a certain type of three-wave mixing) represents an important direction of further research.

We demonstrate that simple and robust single-pass amplifiers based on Cr:ZnS and Cr:ZnSe allow for power scaling of few-optical-cycle pulses to multi-Watt level. We expect that the spinning ring Cr:ZnS and Cr:ZnS laser technology will soon allow us to implement few-cycle MIR sources with 100 W average power at MHz repetition rates.

Availability of high-performance fs sources at 2–3 μm opens several avenues for extension of ultra-fast laser oscillations to the range of 3–20 μm. We demonstrate a very compact and robust MIR source with 10 μJ pulse energy and an octave spanning spectrum (1.6–4.5 μm at -30 dB). The source is based on simultaneous amplification and SCG in a single pass Cr:ZnSe amplifier. Most likely, the obtained output can be re-compressed to sub-two-cycle pulses. Furthermore, we demonstrate that fs Cr:ZnS and Cr:ZnSe lasers represent excellent synchronous pumps for multi-octave OPOs based on a large number of nonlinear materials.

V. Iron Based Lasers

A. Pulsed Operation

As was mentioned in the *Introduction* the lack of high average power convenient pump laser sources between 2.6 and 3.0 μm is one of the challenges in the development of Fe:ZnS/ZnSe MIR lasers operating in the 3.7–5.0 μm spectral range. High average power (20 W) Fe:ZnSe lasers were demonstrated using pulsed HF gas lasers for excitation [87].

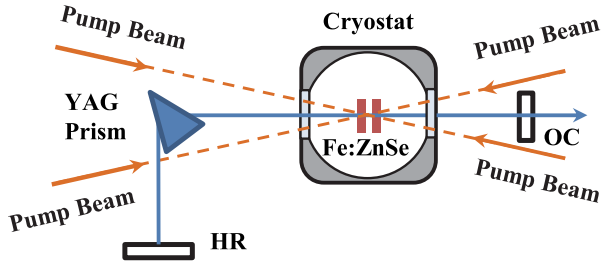

Fig. 32. Optical scheme of tunable Fe:ZnSe laser. HR- high reflector, OC-output coupler.

The power scaling of a pulsed, tunable Fe:ZnSe laser operating at 100 Hz pumped by an Er:YAG laser system was reported in [156]. The free-running oscillation of a flashlamp pumped Er:YAG laser system (oscillation wavelength 2.94 μm and 250 μs pulse duration) based on four laser heads was utilized as a pump source. The maximum repetition rate of the pump laser system was 100 Hz. The maximum pump energy of non-polarized radiation was 1.2 J.

This Fe:ZnSe laser was based on two Fe^{2+} doped ZnSe polycrystals with iron concentration of 1.5×10^{19} cm^{-3}. Doping was accomplished by post-growth thermal diffusion of iron from metal films deposited on crystals grown by chemical vapor transport technique, which were sealed in ampoules under vacuum. The crystals were cut and polished into rectangular slabs with a thickness of 2.00 mm.

The optical scheme of the tunable Fe:ZnSe laser is shown in Fig. 32. Two Fe:ZnSe gain elements were AR coated and mounted at normal incidence to the cavity axis in the liquid nitrogen cryostat. To prevent formation of a strong thermal lens, each of the Fe:ZnSe gain elements was pumped at 50 Hz repetition rate. The best results were obtained in a flat-flat cavity with a 70% output coupler reflectivity using a quasi-collinear pumping scheme. The pump radiation was telescoped by CaF_2 lenses to a beam diameter of $\sim$2 mm at the gain elements. We have used a YAG prism as a dispersive element and the laser wavelength was tuned by rotation of the high reflector.

Staggering of pump pulses from the Er:YAG laser system enabled a 100 Hz repetition rate of the Fe:ZnSe laser with a pulse duration of 150 μs (see Fig. 33). The maximum output power obtained in a nonselective cavity was 35 W operating at 4150 nm under 1.2 J of pump energy per pulse.

The maximum output power obtained in a dispersive cavity was 23 W under 1.0 J of pump energy per pulse. The spectral linewidth measured at 4 μm was equal to 10 nm at FWHM.

This tunable Fe:ZnSe laser operated in TEM_{00} mode (see insert in Fig. 34). The tuning curve over 3.88-4.17 μm spectral region is depicted in Fig. 34. In principle, it is possible to tune this Fe:ZnSe laser up to 5.0 μm. However, in our case tuning over 4.2 μm led to the formation of an intracavity lens due to strong CO_2 absorption, which was accompanied by optical damage of the output coupler.

B. CW Lasers

The first continuous-wave oscillation of an Fe:ZnSe laser at liquid-nitrogen temperature was reported in [75]. Later, 1.6 W

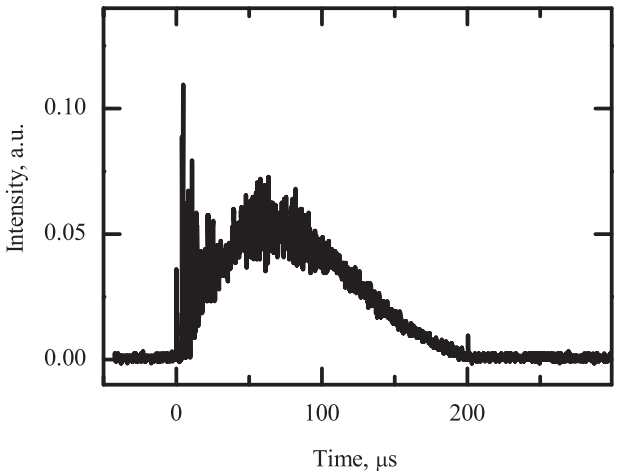

Fig. 33. Temporal profile of Fe:ZnSe laser oscillation at 100 Hz.

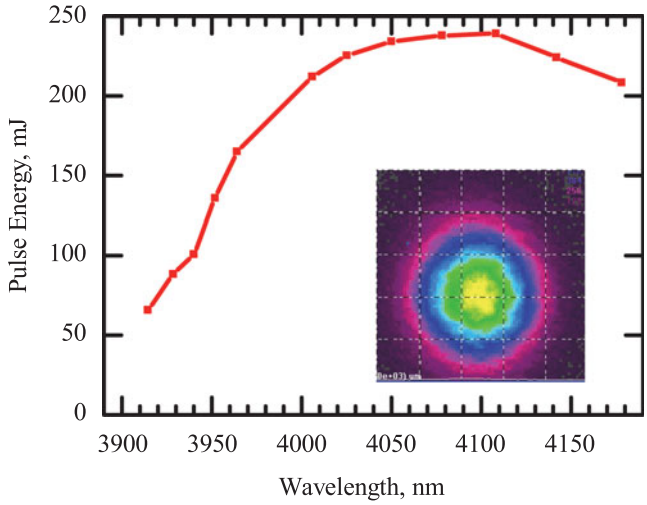

Fig. 34. Tuning curve of Fe:ZnSe laser operating at 100 Hz repletion rate; insert shows and beam profile.

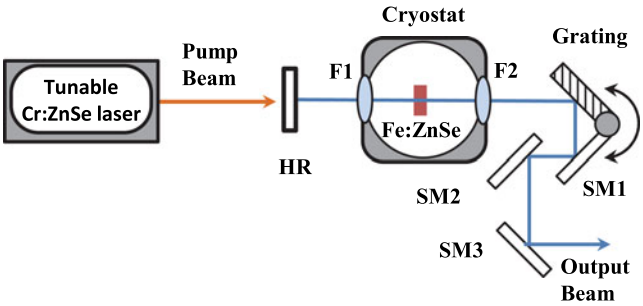

Fig. 35. Optical scheme of CW tunable Fe:ZnSe laser. HR- high reflector, F1, F2 coated CaF_2 intracavity lens, SM gold mirror, SM2, SM3 steering dichroic mirrors.

of output power from a CW Fe:ZnSe laser was demonstrated in a non-selective cavity [28]. The tunable CW oscillation over the 3.7–5.05 μm spectral range and maximum output power exceeding 1 W was demonstrated using the optical scheme depicted in Fig. 35. The laser cavity consists of a simple linear optical resonator formed by a plane high reflector, two lenses and

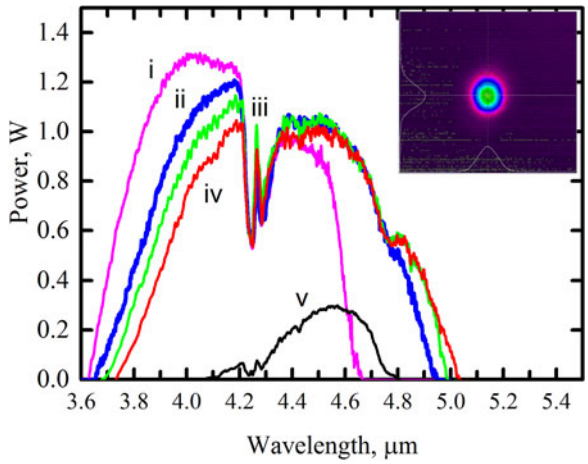

Fig. 36. Tuning curves of Fe:ZnSe laser at different temperatures: (i) 77 K, (ii) 130 K, (iii) 140 K, (iv) 150 K, (v) 160 K.

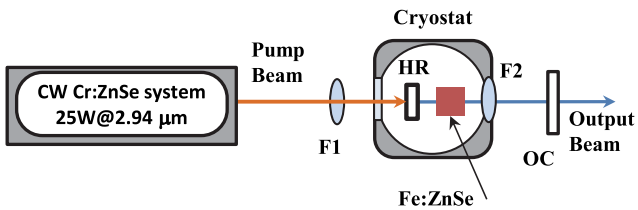

Fig. 37. Optical scheme of CW Fe:ZnSe laser. HR- high reflector, OC – output coupler ~60% reflectivity, F1 – uncoated CaF_2 pump focusing lens f = 25 mm, F2 – uncoated CaF_2 intracavity lens f = 50 mm.

diffraction grating operating in auto-collimation regime (Littrow mounting). The Fe:ZnSe crystal with antireflection coating was placed at normal incident in liquid nitrogen cryostat with a temperature control. The pump was 6 W radiation of a Cr:ZnSe laser operating at 2.8 μm.

Fig. 36 shows a typical tuning curve of narrowline (<0.8 nm) Fe:ZnSe laser operating at different temperatures. A wide dip over the 4.2–4.4 μm spectral range is due to intracavity absorption by atmospheric CO_2 and can be mitigated by cavity purging with Ar or N_2. The maximum oscillation wavelength in this setup was measured to be 5.05 μm.

One of the major problems in development of high power CW Fe:ZnSe lasers has been the absence of high power pump sources overlapping with absorption band of the Fe:ZnSe gain element. The novel approach of thermal management in Cr doped ZnSe/ZnS gain media previously described in Section III-C could be successfully used for development of high power Fe:ZnSe lasers.

In our preliminary experiments, we used the high-power 2940 nm laser system based on the spinning ring Cr:ZnSe gain element with maximum output power of 25 W. The optical scheme of CW Fe:ZnSe laser is shown in Fig. 37. The 2 mm Fe:ZnSe gain elements with iron concentration of 1.5×10^{19} cm^{-3} were AR coated and mounted at normal incidence to the cavity axis in the liquid nitrogen cryostat. The low intensity transmission of the gain element was ~6% at 2.94 μm

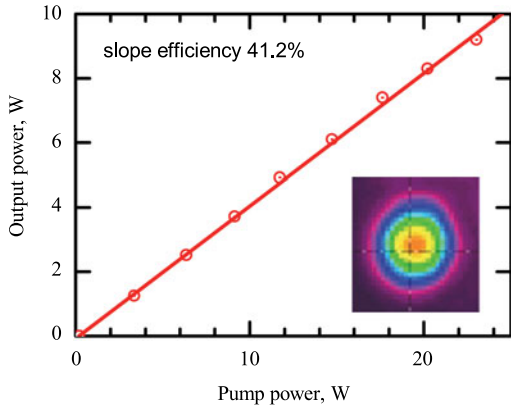

Fig. 38. Input-output characteristics, and beam profile at maximum output power of Fe:ZnSe CW laser operating at 77 °K.

at room temperature and ∼0.4% at 77 K. The pump laser radiation was focused by a CaF_2 lens with a focal distance of f = 25 mm. The laser cavity was formed by a plane high reflection mirror (∼98% reflectivity at 3.9–4.5 μm), uncoated CaF_2 lens f = 50 mm, and a plane output coupler with ∼60% reflectivity. The high reflector was directly placed in the cryostat at ∼1 mm distance from the gain element. The emission of the Fe:ZnSe laser was separated from the residual pump radiation by two dichroic high reflectors (not shown in figure).

The input-output characteristics and beam profile at maximum output power (9.2 W) are depicted in Fig. 38. In spite of intrinsic loses in the laser cavity due to Fresnel reflections of uncoated CaF_2 cryostat windows and uncoated CaF_2 intracavity lens, the lasing threshold was very low - at ∼200 mW of pump radiation. The input-output characteristic had linear dependence with a slope efficiency of ∼41.2%. The laser emission spectrum was relatively broad and centered at 4.15 μm with approximately 100 nm FWHM. The laser was operating in TEM_{00} mode at all the levels of pump power.

VI. Summary and Outlook

Chromium and iron doped ZnSe and ZnS lasers have come of age due to advancements in laser design, thermal management, fabrication of low loss polycrystalline gain media, as well as availability of effective fiber and hybrid fiber-bulk pump lasers. Arguably, Cr and Fe doped ZnSe/S lasers currently represent the most effective route for MIR lasing over the 1.9–5 um spectral range in all the known regimes of oscillation. Important milestones have been reached such as 0.15 kW level of power in pure CW regime; multi-Joule level of output energy in free running and gain-switched regimes of operation; multi-Watt, few-optical cycle ultrafast sources developed.

The future outlook for CW Cr:ZnSe/S lasers is kW output power with hundreds of Watts of output power expected from Fe:ZnSe.

There are several important TM:II-VI material research areas in need of additional studies and improvements. While the developed technology of post-growth thermal diffusion doping enables fabrication of large scale, low loss homogeneously doped Cr:ZnSe/ZnS laser elements, the commercial fabrication of some iron doped II-VI crystals is still in need of additional progress. Another related area of materials research is optimization of hot-press ceramic processing of TM II-VI compounds enabling direct MIR lasing especially at the wavelengths longer than 6 μm. Cd-based binary, ternary, and quaternary chalcogenides are very promising for this application. Favorable spectroscopic characteristics of Fe:CdZnTe microcrystalline powders and the demonstration of RT lasing at 6 μm reported in [58] indicate that these media are promising for solid state laser development with direct lasing at wavelengths longer than 7 μm.

The unique capabilities of polycrystalline Cr:ZnS and Cr:ZnSe for generation, amplification, and nonlinear frequency conversion of ultra-short optical pulses in the MIR range will be further explored for development of octave-spanning single optical cycle oscillators, full repetition rate MOPAs with average power in excess of 100 W, and regenerative amplifiers with tens of mJ levels of output energies. Novel MIR ultrafast sources and frequency combs with exceptional 2–15 μm, spectral span will be developed on the basis of Cr:ZnS/Se based subharmonic OPOs utilizing random phase matching in optical ceramic/polycrystalline materials (e.g., ZnSe [145], ZnS, ZnO, GaN).

The combination of effective MIR Cr:II-VI femtosecond oscillators, the gain media energy storage capabilities of Fe:II-VI which are unique among MIR, and optical parametric and CO_2 amplifiers will be explored for development of Joule-class ultrafast MIR systems operating over the 2–10.6 μm spectral range for high energy physics applications.

Note Added in Proof: The proof-of-principle experiment on the subharmonic thin plate single-crystal ZnSe OPO described in Section IV-D (Fig. 31) was performed in collaboration with Konstantin Vodopyanov, Qitian Ru, and Andrey Muraviev from the University of Central Florida. A comprehensive narrative of the OP-GaAs OPO described in Section IV-D is to be published in the "MIR lasers and applications" special issue of Applied Physics B: V. Smolski, S. Vasilyev, I. Moskalev, M. Mirov, Q. Ru, A. Muraviev, P. Schunemann, S. Mirov, V. Gapontsev, and K. Vodopyanov, "Half-Watt average power femtosecond source spanning 3–8 μm based on subharmonic generation in GaAs," Guest Editors: Wei Ren, Paolo De Natale, Gerard Wysocki, 2018.

Acknowledgment

We are grateful to our colleagues and collaborators: A. Zakrevskiy, S. Klyuyev, D. Cooper, C. Shoemaker, D. Korobeinikov, A. King, J. Poon, F. Stukalin, T. Ness, E. Scherbakov, I. Samartsev, D. Perlov, B. Samson, S. Christensen, A. Markevitch, N. Platonov, M. Meleshkevich, O. Shkurikhin, G. Altshuler, T. King, Y. Kateshov, G. Tsoy, A. Unt, T. Evbatyrov, D. Milyukov, K. Vodopyanov, Q. Ru, A. Muraviev, K. Schepler, P. Berry, J. Goldstein, I. Sorokina, E. Sorokin, R. Camata, O. Gafarov, T. Kesterson, J. Sewell. The work reported here partially involves intellectual property developed at the University of Alabama at Birmingham (UAB). This intellectual property has been licensed to the IPG Photonics Corporation. The UAB coauthors declare competing financial interests.

REFERENCES

[1] W. Low and M. Weger, "Paramagnetic resonance and optical spectra of divalent iron in cubic fields. I. Theory," *Phys. Rev.*, vol. 118, no. 5, pp. 1119–1130, 1960.

[2] J. T. Vallin, G. A. Slack, S. Roberts, and A. E. Hughes, "Infrared absorption in some II-VI compounds doped with Cr," *Phys. Rev. B*, vol. 2, no. 11, pp. 4313–4334, 1970.

[3] H. A. Weakliem, "Optical spectra of Ni^{2+}, Co^{2+}, and Cu^{2+} in tetrahedral sites in crystals," *J. Chem. Phys.*, vol. 36, pp. 2117–2140, 1962.

[4] K. K. Dubenskii, Y. E. Kariss, A. I. Ryskin, P. P. Feofilov, and G. I. Khilko, "Luminescence and absorption associated with the lower terms of Co^{2+} and Ni^{2+} ions in single crystals of ZnS," *Opt. Spectrosc.*, vol. 19, pp. 353–354, 1965.

[5] G. Grebe and H.-J. Schulz, "Luminescence of Cr^{2+} centres and related optical interactions involving crystal field levels of chromium ions in zinc sulfide," *Z. fur Naturforsch.*, vol. 29a, pp. 1803–1819, 1974.

[6] G. A. Slack, F. S. Ham, and R. M. Cherenko, "Optical absorption of tetrahedral Fe^{2+} ($3d^6$) in cubic ZnS, CdTe, and $MgAl_2O_4$," *Phys. Rev.*, vol. 152, pp. 376–402, 1966.

[7] R. Renz and H.-J. Schulz, "The decay of infrared luminescence in II-VI compound semiconductors doped by 3D transition elements," *J. Phys. C, Solid State Phys.*, vol. 16, pp. 4917–4932, 1983.

[8] L. Podlowski, R. Heitz, P. Thurian, A. Hoffmann, and I. Broser, "Non-radiative transition rates of Fe^{2+} in III–V and II–VI semiconductors," *J. Lumin.*, vol. 58, pp. 252–256, 1994.

[9] L. D. DeLoach, R. H. Page, G. D. Wilke, S. A. Payne, and W. F. Krupke, "Transition metal-doped zinc chalcogenides: Spectroscopy and laser demonstration of a new of gain media," *IEEE J. Quantum Electron.*, vol. 32, no. 6, pp. 885–895, Jun. 1996.

[10] R. H. Page *et al.*, "Cr^{2+}-doped sinc chalcogenides as efficient, widely tunable mid-infrared lasers," *IEEE J. Quantum Electron.*, vol. 33, no. 4, pp. 609–619, Apr. 1997.

[11] D. C. Harris, "Development of hot-pressed and chemical-vapor-deposited zinc sulfide and zinc selenide in the United States for optical windows," *Proc. SPIE*, vol. 6545, May 2, 2007, Art. no. 654502.

[12] A. V. Podlipensky *et al.*, "Pulsed laser operation of diffusion-doped Cr:ZnSe," *Opt. Commun.*, vol. 167, pp. 129–132, 1999.

[13] K. Graham *et al.*, "Spectroscopic characterization and laser performance of diffusion doped Cr^{2+}:ZnS," in *OSA Trends in Optics and Photonics on Advanced Solid State Lasers*, vol. 46, S. Payne and C. Marshall, Eds. Washington, DC, USA: Optical Society of America, 2001, pp. 561–567.

[14] A. Burger *et al.*, "Preparation conditions of chromium doped ZnSe and their infrared luminescence properties," *J. Cryst. Growth*, vol. 225, pp. 249–256, 2001.

[15] J.-O. Ndap, K. Chattopadhyay, O. O. Adetunji, D. E. Zelmon, and A. Burger, "Thermal diffusion of Cr^{2+} in bulk ZnSe," *J. Cryst. Growth*, vol. 240, pp. 176–184, 2002.

[16] S. B. Mirov *et al.*, "Diode and fiber pumped Cr^{2+}:ZnS mid-IR external cavity and microchip lasers," *IEE Optoelectron.*, vol. 150, no. 4, pp. 340–345, 2003.

[17] U. Demirbas, A. Sennaroglu, and M. Somer, "Synthesis and characterization of diffusion-doped Cr^{2+}:ZnSe and Fe^{2+}:ZnSe," *Opt. Mater.*, vol. 28, pp. 231–240, 2006.

[18] S. Kück, "Laser-related spectroscopy of ion-doped crystals for tunable solid-state lasers," *Appl. Phys. B*, vol. 72, pp. 515–562, 2001.

[19] S. Kück, "Spectroscopy and laser characteristics of Cr -doped chalcogenide crystals—Overview and recent results" *J. Alloys Compounds*, vol. 341, pp. 28–33, 2002.

[20] T. J. Carrig, "Transition-metal-doped chalcogenide lasers," *J. Electron. Mater.*, vol. 31, pp. 759–769, 2002.

[21] A. G. Bluiett *et al.*, "Observation of lasing from Cr^{2+}:CdTe and compositional effects in Cr^{2+}-doped II-VI semiconductors," *J. Electron. Mater.*, vol. 31, no. 7, pp. 806–810, 2002.

[22] E. Sorokin, S. Naumov, and I. T. Sorokina, "Ultrabroadband infrared solid state lasers," *IEEE J. Sel. Topics Quantum Electron.*, vol. 11, no. 3, pp. 690–712, May/Jun. 2005.

[23] S. Mirov, V. Fedorov, I. Moskalev, and D. Martyshkin, "Recent progress in transition metal doped II-VI mid-IR lasers" *IEEE J. Sel. Topics Quantum Electron.*, vol. 13, no. 3, pp. 810–822, May/Jun. 2007.

[24] A. Sennaroglu and U. Demibras, "Tunable Cr^{2+}:ZnSe lasers in the mid-infrared," in *Solid State Lasers and Applications*, A. Sennaroglu, Ed. Boca Raton, FL, USA: CRC Press, 2007, pp. 113–162.

[25] S. Mirov, V. Fedorov, I. S. Moskalev, D. Martyshkin, and C. Kim, "Progress in Cr^{2+} and Fe^{2+} doped mid-IR laser materials," *Laser Photon. Rev.*, vol. 4, no. 1, pp. 21–41, 2010.

[26] V. I. Kozlovsky *et al.*, "Room-temperature tunable mid-infrared lasers on transition-metal doped II–VI compound crystals grown from vapor phase," *Phys. Status Solidi B*, vol. 247, no. 6, pp. 1553–1556, 2010.

[27] S. Mirov, V. Fedorov, I. Moskalev, M. Mirov, and D. Martyshkin, "Frontiers of mid-infrared lasers based on transition metal doped II–VI semiconductors," *J. Lumin.*, vol. 133, pp. 268–275, 2013.

[28] S. Mirov *et al.*, "Progress in mid-IR lasers based on Cr and Fe doped II-VI chalcogenides," *IEEE J. Sel. Topics Quantum Electron.*, vol. 21, no. 1, Jan./Feb. 2015, Art. no. 1601719.

[29] V. I. Kozlovsky, Y. V. Korostelin, Y. P. Podmar'kov, Y. K. Skasyrsky, and M. P. Frolov, "Middle infrared Fe^{2+}:ZnS, Fe^{2+}:ZnSe and Cr^{2+}:CdSe lasers: New results," *J. Phys., Conf. Ser.*, vol. 740, no. 1, pp. 1–6, 2016.

[30] A. M. Malyarevich and K. V. Yumashev, "Saturable absorbers based on tetrahedrally coordinated transition-metal ions in crystals (review)," *J. Appl. Spectrosc.*, vol. 76, pp. 1–43, 2009.

[31] N. Myoung, V. V. Fedorov, S. B. Mirov, and L. E. Wenger, "Temperature and concentration quenching of mid-IR photoluminescence in iron doped ZnSe and ZnS laser crystals," *J. Lumin.*, vol. 132, no. 3, pp. 600–606, 2012.

[32] J. J. Adams *et al.*, "4.0–4.5 um lasing of Fe:ZnSe below 180, a new mid-infrared laser material," *Opt. Lett.*, vol. 24, no. 3, pp. 1720–1722, 1999.

[33] V. V. Fedorov, T. Konak, J. Dashdorj, M. E. Zvanut, and S. B. Mirov, "Optical and EPR spectroscopy of Zn:Cr:ZnSe and Zn:Fe:ZnSe crystals," *Opt. Mater.*, vol. 37, pp. 262–266, 2014.

[34] M. Mond *et al.*, "Erbium doped fibre amplifier pumped Cr^{2+}:ZnSe laser," *Phys. Status Solidi. A*, vol. 188, no. 4, pp. R3–R5, 2001.

[35] I. T. Sorokina *et al.*, "Continuous-wave tunable Cr^{2+}:ZnS laser," *Appl. Phys. B.*, vol. 74, pp. 607–611, 2002.

[36] A. Zakel *et al.*, "High-brightness, rapidly-tunable Cr:ZnSe lasers," in *Proc. Adv. Solid-State Photon.*, 2005, Paper MD2.

[37] J. T. Seo, U. Hommerich, S. B. Trivedi, R. J. Chen, and S. Kutcher, "Slope efficiency and tunability of a Cr^{2+}:CdMnTe mid-infrared laser," *Opt. Commun.*, vol. 153, pp. 267–270, 1998.

[38] J. McKay, K. L. Schepler, and G. C. Catella, "Efficient grating-tuned mid-infrared Cr^{2+}:CdSe laser," *Opt. Lett.*, vol. 24, pp. 1575–1577, 1999.

[39] U. Hommerich *et al.*, "Demonstration of room-temperature laser action at 2.5 mm from Cr^{2+}:$Cd_{0.85}Mn_{0.15}Te$," *Opt. Lett.*, vol. 22, pp. 1180–1182, 1997.

[40] A. Sennaroglu, A. O. Konca, and C. R. Pollock, "Continuous-wave power performance of a 2.47-μm Cr^{2+}:ZnSe laser: Experiment and modeling," *IEEE J. Quantum Electron.*, vol. 36, no. 10, pp. 1199–1205, Oct. 2000.

[41] K. Graham *et al.*, "Pulsed mid-IR Cr^{2+}:ZnS and Cr^{2+}:ZnSe lasers pumped by Q-switched neodymium Raman lasers," *Quantum Electron.*, vol. 34, no. 1, pp. 8–14, 2004.

[42] R. H. Page *et al.*, "Demonstrations of diode-pumped and grating-tuned. ZnSe:Cr^{2+} lasers," in *Trends in Optics and Photonics, Advanced Solid State Lasers*, C. R. Pollock and W. R. Bosenberg, Eds. vol. 10, Washington, D.C., USA: Optical Society of America, 1997, pp. 208–210.

[43] G. J. Wagner, A. Schober, G. Bennett, J. Marquardt, and T. Carrig, "Multi-watt broadly-tunable diode-pumped Cr:ZnSe laser," in *Proc. Conf. Lasers Electro-Opt.*, 2012, Art. no. CTu2D.2.

[44] V. V. Fedorov, A. Gallian, I. Moskalev, and S. B. Mirov, "En route to electrically pumped broadly tunable middle infrared lasers based on transition metal doped II–VI semiconductors," *J. Lumin.*, vol. 125, no. 1/2, pp. 184–195, 2007.

[45] J. Peppers, V. V. Fedorov, and S. B. Mirov, "Mid-IR Photoluminescence of Fe^{2+} and Cr^{2+} ions in ZnSe crystal under excitation in charge transfer bands," *Opt. Express*, vol. 23, no. 4, pp. 4406–4414, 2015.

[46] G. J. Wagner *et al.*, "Continuous-wave broadly tunable Cr^{2+}:ZnSe laser," *Opt. Lett.*, vol. 24, pp. 19–21, 1999.

[47] I. Moskalev *et al.*, "140 W Cr:ZnSe laser system," *Opt. Express*, vol. 24, pp. 21090–21104, 2016.

[48] D. N. Nikogosyan, *Properties of Optical and Laser-Related Materials: A Handbook*. Hoboken, NJ, USA: Wiley, 1997.

[49] S. Adachi, *Properties of Group-IV, III-V and II-VI Semiconductors*. Hoboken, NJ, USA: Wiley, 2005.

[50] S. Adachi, *Handbook on Physical Properties of Semiconductors: Volume 3 III-V Compound Semiconductors*. Boston, MA, USA: Kluwer, 2004.

[51] I. T. Sorokina, "Cr^{2+}-doped II–VI materials for lasers and nonlinear optics," *Opt. Mater.*, vol. 26, pp. 395–412, 2004.

[52] E. Sorokin *et al.*, "Continuous-wave broadly tunable high-power Cr:CdS laser," *Appl. Phys. B*, vol. 117, pp. 1009–1014, 2014.

[53] S. B. Mirov *et al.*, "Progress in mid-IR Cr^{2+} and Fe^{2+} doped II-VI materials and lasers [Invited]," *Opt. Mater. Express*, vol. 1, pp. 898–910, 2011.

[54] J. McKay, W. B. Roh, and K. L. Schepler, "Extended Mid-IR tuning of a Cr^{2+}:CdSe Laser," *OSA Trends Opt. Photon.*, vol. 68, pp. 371–373, 2002.

[55] M. P. Frolov *et al.*, "Fe^{2+}-doped CdSe single crystal: Growth, spectroscopic and laser properties, potential use as a 6 μm broadband amplifier," *Laser Phys. Lett.*, vol. 14, 2017, Art. no. 025001.

[56] G. A. Slack, S. Roberts, and J. T. Vallin, "Optical absorption of Fe^{2+} in CdTe in the near and far infrared," *Phys. Rev.*, vol. 187, pp. 511–524, 1969.

[57] R. Pappalardo and R. E. Dietz, "Absorption spectra of transition ions in CdS crystals," *Phys. Rev.*, vol. 123, pp. 1188–1203, 1961.

[58] A. D. Martinez, D. V. Martyshkin, R. P. Camata, V. V. Fedorov, and S. B. Mirov, "Crystal field engineering of transition metal doped II-VI ternary and quaternary semiconductors for mid-IR tunable laser applications," *Opt. Mater. Express*, vol. 5, pp. 2036–2046, 2015.

[59] V. Fedorov *et al.*, "Compact 1J mid-IR Cr:ZnSe laser," in *Proc. Front. Opt.*, Rochester, NY, USA, 2012, Paper FW6B.9.

[60] V. V. Fedorov *et al.*, "Energy scaling of nanosecond gain-switched Cr^{2+}:ZnSe lasers," *Proc. SPIE*, vol. 7912, 2011, Art. no. 79121E.

[61] M. Yumoto, N. Saito, U. Takagi, T. Tomida, and S. Wada, "Multi-stage Cr:ZnSe power amplifier pumped with Q-switched Tm:YAG laser," in *Proc. Conf. Lasers Electro-Opt.*, 2013, Paper CTu3D.2.

[62] T. J. Carrig, G. J. Wagner, A. Sennaroglu, J. Y. Jeong, and C. R. Pollock, "Mode-locked Cr^{2+}:ZnSe laser," *Opt. Lett.*, vol. 25, pp. 168–170, 2000.

[63] I. Sorokina *et al.*, "Active and passive mode-locking of Cr^{2+}:ZnSe laser," in *Proc. Adv. Solid-State Lasers*, Seattle,WA, USA, 2001, Paper MC2.

[64] C. Pollock *et al.*, "Mode locked and Q-switched Cr:ZnSe laser using a semiconductor saturable absorbing mirror (SESAM)," in *Proc. Adv. Solid-State Photon.*, Vienna, Austria, 2005, Paper TuA6.

[65] I. T. Sorokina, E. Sorokin, and T. Carrig, "Femtosecond pulse generation from a SESAM mode-locked Cr:ZnSe laser," in *Proc. Conf. Lasers Electro-Opt./Quantum Electron. Laser Sci. Conf. Photon. Appl. Syst. Technol.*, Paper CMQ2.

[66] U. Hommerich *et al.*, "Mid-infrared laser development based on transition metal doped cadmium manganese telluride," *J. Lumin.*, vol. 87, pp. 1143–1145, 2000.

[67] V. A. Akimov *et al.*, "Pulsed broadly tunable room-temperature Cr^{2+}:CdS laser," *Appl. Phys. B*, vol. 97, 793–797, 2009.

[68] E. V. Sorokin *et al.*, "Spectroscopy and tunable continuous-wave operation of Cr^{2+}:$Zn_{1-x}Mg_xSe$ single crystal around 2.5 μm," *Quantum Electron.*, vol. 45, no. 4, pp. 301–304, 2015.

[69] M. E. Doroshenko *et al.*, "Cr:ZnMgSe laser pumped by 1.7 μm Er:YLF radiation," *Proc. SPIE* vol. 8599, 2013, Art. no. 859921.

[70] U. Demirbas and A. Sennaroglu, "Intracavity-pumped Cr^{2+}:ZnSe laser with ultrabroadband tuning range between 1880 and 3100 nm," *Opt. Lett.*, vol. 31, pp. 2293–2295, 2006.

[71] V. A. Akimov *et al.*, "Efficient pulsed Cr^{2+}:CdSe laser continuously tunable in the spectral range from 2.26 to 3.61 μm," *Quantum Electron.*, vol. 38, no. 3, pp. 205–208, 2008.

[72] G. J. Wagner *et al.*, "High-efficiency, broadly tunable continuous-wave Cr^{2+}:ZnSe laser," in *Trends Optics Photon. Adv. Solid State Lasers*, M. M. Fejer, H. Injeyan, U. Keller, Eds. vol. 26,Washington DC, USA: Optical Society of America, 1999, pp. 427–434.

[73] M. N. Cizmeciyan, H. Cankaya, A. Kurt, and A. Sennaroglu, "Kerr-lens mode-locked femtosecond Cr^{2+}:ZnSe laser at 2420 nm," *Opt. Lett.*, vol. 34, pp. 3056–3058, 2009.

[74] P. B. Klein, J. E. Furneaux, and R. L. Henry, "Laser oscillation at 3.53 μm from Fe^{2+} in n-InP:Fe," *Appl. Phys. Lett.*, vol. 42, pp. 638–640, 1983.

[75] A. A. Voronov *et al.*, "A continuous-wave Fe^{2+}:ZnSe laser," *Quantum Electron.*, vol. 38, no. 12, pp. 1113–1116, 2008.

[76] J. Kernal, V. V. Fedorov, A. Gallian, S. B. Mirov, and V. Badikov, "3.9-4.8 μm gain-switched lasing of Fe:ZnSe at room temperature," *Opt. Express*, vol. 13, no. 26, pp. 10608–10615, 2005.

[77] V. I. Kozlovsky *et al.*, "Pulsed Fe^{2+}:ZnS laser continuously tunable in the wavelength range of 3.49–4.65 μm," *Quantum Electron.*, vol. 41, pp. 1–3, 2011.

[78] M. P. Frolov *et al.*, "Fe^{2+}-doped CdSe single crystal: Growth, spectroscopic and laser properties, potential use as a 6 μm broadband amplifier," *Laser Phys. Lett.*, vol. 14, 2017, Art. no. 025001.

[79] S. D. Velikanov *et al.*, "Fe^{2+}:ZnSe laser pumped by a non-chain electric-discharge HF laser at room temperature," *Quantum Electron.*, vol. 44, no. 2, pp. 141–144, 2014.

[80] N. Myoung, D. V. Martyshkin, V. V. Fedorov, and S. B. Mirov, "Mid-IR lasing of iron–cobalt co-doped ZnS(Se) crystals via Co–Fe energy transfer," *J. Lumin.*, vol. 133, pp. 257–261, 2013.

[81] J. M. Peppers, D. V. Martyshkin, V. V. Fedorov, and S. B. Mirov, "Spectroscopic characterization and energy transfer process in cobalt and cobalt-iron co-doped ZnSe/ZnS crystals," *Proc. SPIE*, vol. 8959, 2014, pp. 8959–8962.

[82] V. A. Akimov *et al.*, "Efficient IR Fe:ZnSe laser continuously tunable in the spectral range from 3.77 to 4.40 μm," *Quantum Electron.*, vol. 34, no. 10, pp. 912–914, 2004.

[83] V. V. Fedorov *et al.*, "3.77–5.05-mm tunable solid-state lasers based on Fe^{2+}-doped ZnSe crystals operating at low and room temperatures," *IEEE J. Quantum Electron.*, vol. 42, no. 9, pp. 907–917, Sep. 2006.

[84] M. E. Doroshenko *et al.*, "Spectroscopic and laser properties of bulk iron doped zinc magnesium selenide Fe:ZnMgSe generating at 4.5–5.1 μm," *Opt. Express*, vol. 24, pp. 19824–19834, 2016.

[85] S. D. Velikanov *et al.*, "Investigation of Fe:ZnSe laser in pulsed and repetitively pulsed regimes," *Quantum Electron.*, vol. 45, no. 1, pp. 1–7, 2004.

[86] D. V. Martyshkin *et al.*, "High power (9.2 W) CW 4.15 μm Fe:ZnSe laser," in *Proc. Conf. Lasers Electro-Opt.*, 2017, Paper STh1L.6.

[87] S. D. Velikanov *et al.*, "Repetitively pulsed Fe:ZnSe laser with an average output power of 20 W at room temperature of the polycrystalline active element," *Quantum Electron.*, vol. 47, no. 4, pp. 303–307, 2017.

[88] A. E. Dormidonov *et al.*, "High-efficiency room-temperature ZnSe:Fe^{2+} laser with a high pulsed radiation energy," *Appl. Phys. B*, vol. 122, no. 8, 2016, Art. no. 211.

[89] D. J. Richardson, J. Nilsson, and W. A. Clarkson, High power fiber lasers: Current status and future perspectives (invited)," *J. Opt. Soc. Amer. B*, vol. 27, no. 11, pp. B63–B92, 2010.

[90] S. A. Payne, L. L. Chase, L. K. Smith, W. L. Kway, and W. F. Krupke, "Infrared cross-section measurements for crystals doped with Er^{3+}, Tm^{3+}, and Ho^{3+}," *IEEE J. Quantum Electron.*, vol. 28, no. 11, pp. 2619–2630, Nov. 1992.

[91] D. Y. Shen, J. K. Sahu, and W. A. Clarkson, "Highly efficient in-band pumped Er:YAG laser with 60 W of output at 1645 nm," *Opt. Lett.*, vol. 31, pp. 754–756, 2006.

[92] S. D. Setzler, M. P. Francis, Y. E. Young, J. R. Konves, and E. P. Chicklis, "Resonantly pumped eyesafe erbium lasers," *IEEE J. Sel. Topics Quantum Electron.*, vol. 11, no. 3, pp. 645–657, May/Jun. 2005.

[93] J. W. Kim, D. Y. Shen, J. K. Sahu, and W. A. Clarkson, "Fiber-laser-pumped Er:YAG lasers," *IEEE J. Sel. Topics Quantum Electron.*, vol. 15, no. 2, pp. 361–371, Mar./Apr. 2009.

[94] C. Larat, M. Schwarz, E. Lallier, and E. Durand, "120 mJ Q-switched Er:YAG laser at 1645 nm," *Opt. Express*, vol. 22, pp. 4861–4866, 2014.

[95] Z. Yu, M. Wang, X. Hou, and W. Chen, "High-energy resonantly diode-pumped Q-switched Er:YAG laser at 1617 nm," *Appl. Phys. B*, vol. 122, no. 4, pp. 84–90, 2016.

[96] K. Schmidt, C. Reiter, H. Voss, F. Maßmann, and M. Ostermeyer, "High energy 125mJ Ho:YAG (2.09 μm) MOPA double pass laser system pumped by cw thulium fiber laser (1.9 μm)," presented at the Conf. Lasers Electro-Opt. Eur. 12th Eur. Quantum Electron. Conf., Munich, Germany, 2011.

[97] K. K. Yu, X. M. Duan, D. X. Zhang, B. Q. Yao, and Y. J. Shen, "A 1 kHz, 30 mJ Ho:YAG master oscillator and power amplifier resonantly double-end-pumped by Tm:YLF lasers," *Laser Phys.*, vol. 23, no. 6, 2013, Art. no. 065001.

[98] X. M. Duan *et al.*, "A dual-end-pumped Ho:YAG laser with a high energy output," *Quantum Electron.*, vol. 45, no. 8, pp. 701–703, 2015.

[99] A. Dergachev, D. Armstrong, A. Smith, T. Drake, and M. Dubois, "3.4-μm ZGP RISTRA nanosecond optical parametric oscillator pumped by a 2.05-μm Ho:YLF MOPA system," *Opt. Express*, vol. 15, pp. 14404–14413, 2007.

[100] A. Dergachev, D. Armstrong, A. Smith, T. E. Drake, and M. Dubois, "High-power, high-energy ZGP OPA pumped by a 2.05-μm Ho:YLF MOPA system," *Proc. SPIE*, vol. 6875, pp. 687507-1–687507-10, 2008.

[101] E. Sorokin *et al.*, "Ultrabroad continuous-wave tuning of ceramic Cr:ZnSe and Cr:ZnS lasers," in *Proc. Adv. Solid-State Photon.*, 2010, Paper AMC2.

[102] J. McKay, W. Roh, and K. Schepler, "Thermal lensing in Cr^{2+}:ZnSe face-cooled disks," in *Proc. Advanced Solid-State Photon.*, vol. 83, 2003, Paper 220.

[103] H. Krol, C. Grèzes-Besset, L. Gallais, J. Natoli, and M. Commandré, "Study of laser-induced damage at 2 microns on coated and uncoated ZnSe substrates," *Proc. SPIE*, vol. 6403, 2006, Art. no. 640316.

[104] S. McDaniel *et al.*, "Cr:ZnSe laser incorporating anti-reflection microstructures exhibiting low-loss, damage-resistant lasing at near quantum limit efficiency," *Opt. Mater. Express*, vol. 4, pp. 2225–2232, 2014.

[105] C. Pollock *et al.*, "Mode locked and Q-switched Cr:ZnSe laser using a semiconductor saturable absorbing mirror (SESAM)," in *Proc. Adv. Solid-State Photon.*, 2005, Paper TuA6.

[106] P. Moulton and E. Slobodchikov, "1-GW-peak-power, Cr:ZnSe laser," in *Proc. Conf. Lasers Electro-Opt.*, 2011, Paper PDPA10.

[107] M. N. Cizmeciyan *et al.*, "Graphene mode-locked femtosecond Cr:ZnSe laser at 2500 nm," *Opt. Lett.*, vol. 38, no. 3, pp. 341–343, 2013.

[108] I. T. Sorokina and E. Sorokin, "Femtosecond Cr^{2+} -based lasers," *IEEE J. Sel. Topics Quantum Electron.*, vol. 21, no. 1, Art. no. 1601519, Jan./Feb. 2015.

[109] E. Slobodchikov, L. R. Chieffo, and K. F. Wall, "High peak power ultrafast Cr:ZnSe oscillator and power amplifier," *Proc. SPIE*, vol. 9726, Mar. 16, 2016, Art. no. 972603.

[110] N. Tolstik, E. Sorokin, and I. T. Sorokina, "Graphene mode-locked Cr:ZnS laser with 41 fs pulse duration," *Opt. Express*, vol. 22, no. 5, pp. 5564–5571, 2014.

[111] N. Tolstik, E. Sorokin, and I. T. Sorokina, "Gigahertz femtosecond Cr:ZnS laser," in *Proc. Adv. Solid-State Lasers*, 2014, Paper AM3A.1.

[112] E. Sorokin, N. Tolstik, K. I. Schaffers, and I. T. Sorokina, "Femtosecond SESAM-modelocked Cr:ZnS laser," *Opt. Express*, vol. 20, pp. 28947–28952, 2012.

[113] M. N. Cizmeciyan, H. Cankaya, A. Kurt, and A. Sennaroglu, "Operation of femtosecond Kerr-lens mode-locked Cr:ZnSe lasers with different dispersion compensation methods," *Appl. Phys. B*, vol. 106, pp. 887–892, 2012.

[114] N. Tolstik, E. Sorokin, and I. T. Sorokina, "Kerr-lens mode-locked Cr:ZnS laser," *Opt. Lett.*, vol. 38, pp. 299–301, 2013.

[115] E. Sorokin, N. Tolstik, and I. T. Sorokina, "1 Watt femtosecond mid-IR Cr:ZnS laser," *Proc. SPIE*, vol. 8599, Mar. 2013, Art. no. 859916.

[116] S. Vasilyev, M. Mirov, and V. Gapontsev, "Kerr-lens mode-locked femtosecond polycrystalline Cr^{2+}:ZnS and Cr^{2+}:ZnSe lasers," *Opt. Express* vol. 22, no. 5, pp. 5118–5123, 2014.

[117] S. Vasilyev, I. Moskalev, M. Mirov, S. Mirov, and V. Gapontsev, "Three optical cycle mid-IR Kerr-lens mode-locked polycrystalline Cr^{2+}:ZnS laser," *Opt. Lett.*, vol. 40, pp. 5054–5057, 2015.

[118] S. Vasilyev, M. Mirov, and V. Gapontsev, "Mid-IR Kerr-lens mode-locked polycrystalline Cr^{2+}:ZnS laser with 0.5 MW peak power," in *Proc. Adv. Solid-State Lasers*, 2015, Paper AW4A.3.

[119] S. Vasilyev *et al.*, "Kerr-lens mode-locked middle IR polycrystalline Cr:ZnS laser with a repetition rate 1.2 GHz," in *Proc. Lasers Congr. 2016 (ASSL, LSC, LAC)*, 2016, Paper AW1A.2.

[120] S. Vasilyev, I. Moskalev, M. Mirov, S. Mirov, and V. Gapontsev, "Multi-watt mid-IR femtosecond polycrystalline Cr^{2+}:ZnS and Cr^{2+}:ZnSe laser amplifiers with the spectrum spanning 2.0–2.6 μm," *Opt. Express*, vol. 24, pp. 1616–1623, 2016.

[121] S. Vasilyev *et al.*, "Ultrafast middle-IR lasers and amplifiers based on polycrystalline Cr:ZnS and Cr:ZnSe," *Opt. Mater. Express*, vol. 7, pp. 2636–2650, 2017.

[122] M. Durand *et al.*, "Study of filamentation threshold in zinc selenide," *Opt. Express*, vol. 22, no. 5, pp. 5852–5858, 2014.

[123] H. Liang *et al.*, "Three-octave-spanning supercontinuum generation and sub-two-cycle self-compression of mid-infrared filaments in dielectrics," *Opt. Lett.*, vol. 40, no. 6, pp. 1069–1072, 2015.

[124] O. Mouawad *et al.*, "Filament-induced visible-to-mid-IR supercontinuum in a ZnSe crystal: Towards multi-octave supercontinuum absorption spectroscopy," *Opt. Mater.*, vol. 60, pp. 355–358, 2016.

[125] R. Suminas *et al.*, "Multi-octave spanning nonlinear interactions induced by femtosecond filamentation in polycrystalline ZnSe," *Appl. Phys. Lett.*, vol. 110, 2017, Art. no. 241106.

[126] A. Dubietis, G. Tamošauskas, R. Šuminas, V. Jukna, and A. Couairon, "Ultrafast supercontinuum generation in bulk condensed media," *Lith. J. Phys.*, vol. 57, no. 3, pp. 113–157, 2017.

[127] H. P. Wagner, M. Kühnelt, W. Langbein, and J. M. Hvam, "Dispersion of the second-order nonlinear susceptibility in ZnTe, ZnSe, and ZnS," *Phys. Rev. B*, vol. 58, no. 16, pp. 10494–10501, 1998.

[128] I. Shoji, T. Kondo, A. Kitamoto, M. Shirane, and R. Ito, "Absolute scale of second-order nonlinear-optical coefficients," *J. Opt. Soc. Amer. B*, vol. 14, no. 9, pp. 2268–2294, 1997.

[129] E. Y. Morozov, A. A. Kaminskii, A. S. Chirkin, and D. B. Yusupov, "Second optical harmonic generation in nonlinear crystals with a disordered domain structure," *JETP Lett*., vol. 73, no. 12, pp. 647–650, 2001.

[130] E. Y. Morozov and A. S. Chirkin, "Stochastic quasi-phase matching in nonlinear-optical crystals with an irregular domain structure," *Quantum Electron.*, vol. 34, no. 3, pp. 227–232, 2004.

[131] M. Baudrier-Raybaut, R. Haïdar, P. Kupecek, P. Lemasson, and E. Rosencher, "Random quasi-phase-matching in bulk polycrystalline isotropic nonlinear materials," *Nature*, vol. 432, pp. 374–376, 2004.

[132] S. Vasilyev, M. Mirov, and V. Gapontsev, "High power Kerr-lens mode-locked femtosecond mid-IR laser with efficient second harmonic generation in polycrystalline Cr^{2+}:ZnS and Cr^{2+}:ZnSe," in *Proc. Adv. Solid State Lasers*, 2014, Paper AM3A.3.

[133] S. Vasilyev *et al.*, "Mid-IR Kerr-lens mode-locked polycrystalline Cr:ZnS and Cr:ZnSe lasers with intracavity frequency conversion via random quasi-phase-matching," *Proc. SPIE*, vol. 9731, Mar. 2016, Art. no. 97310B.

[134] A. Schliesser, N. Picqué, and T. W. Hänsch, "Mid-infrared frequency combs," *Nature Photon.*, vol. 6, pp. 440–449, 2012.

[135] A. Gambetta *et al.*, "Milliwatt-level frequency combs in the 8–14 μm range via difference frequency generation from an Er:Fiber oscillator," *Opt. Lett.*, vol. 38, pp. 1155–1157, 2013.

[136] G. Soboń, T. Martynkien, P. Mergo, L. Rutkowski, and A. Foltynowicz, "High-power frequency comb source tunable from 2.7 to 4.2 μm based on difference frequency generation pumped by an Yb-doped fiber laser," *Opt. Lett.*, vol. 42, pp. 1748–1751, 2017.

[137] I. Pupeza *et al.*, "High-power sub-two-cycle mid-infrared pulses at 100 MHz repetition rate," *Nature Photon.*, vol. 9, pp. 721–724, 2015.

[138] T. Morimoto, N. Sono, T. Miyamoto, N. Kida, and H. Okamoto, "Generation of a carrier-envelope-phase-stable femtosecond pulse at 10 μm by direct down-conversion from a Ti:Sapphire laser pulse," *Appl. Phys. Express*, vol. 10, 2017, Art. no. 122701.

[139] S. T. Wong, K. L. Vodopyanov, and R. L. Byer, "Self-phase-locked divide-by-2 optical parametric oscillator as a broadband frequency comb source," *J. Opt. Soc. Amer. B*, vol. 27, pp. 876–882, 2010.

[140] V. O. Smolski, H. Yang, S. D. Gorelov, P. G. Schunemann, and K. L. Vodopyanov, "Coherence properties of a 2.6–7.5 μm frequency comb produced as a subharmonic of a Tm-fiber laser," *Opt. Lett.*, vol. 41, pp. 1388–1391, 2016.

[141] K. L. Vodopyanov, E. Sorokin, I. T. Sorokina, and P. G. Schunemann, "Mid-IR frequency comb source spanning 4.4–5.4 μm based on subharmonic GaAs optical parametric oscillator," *Opt. Lett.*, vol. 36, pp. 2275–2277, 2011.

[142] B. Bernhardt *et al.*, "Mid-infrared dual-comb spectroscopy with 2.4 μm Cr^{2+}:ZnSe femtosecond lasers," *Appl. Phys. B*, vol. 100, pp. 3–8, 2010.

[143] Q. Ru *et al.*, "Instantaneous spectral span of 2.85-8.40 μm achieved in a Cr:ZnS laser pumped subharmonic OPO," *Proc. SPIE*, vol. 10088, 2017, Art. no. 1008809.

[144] V. O. Smolski, S. Vasilyev, P. G. Schunemann, S. B. Mirov, and K. L. Vodopyanov, "Cr:ZnS laser-pumped subharmonic GaAs optical parametric oscillator with the spectrum spanning 3.6–5.6 μm," *Opt. Lett.*, vol. 40, pp. 2906–2908, 2015.

[145] Q. Ru *et al.*, "Optical parametric oscillation in a random polycrystalline medium (memorandum)," *Optica*, vol. 4, no. 6, 617–618, Jun. 2017.

[146] Y. Wang *et al.*, "47-fs Kerr-lens mode-locked Cr:ZnSe laser with high spectral purity," *Opt. Express*, vol. 25, pp. 25193–25200, 2017.

[147] J. Zhang *et al.*, "Generation of 220 fs, 20 W pulses at 2 μm from Kerr-lens mode-locked Ho:YAG thin-disk oscillator," in *Proc. Conf. Lasers Electro-Opt.*, 2017, Paper SM1I.6.

[148] J. Zhang *et al.*, "7-W, 2-cycle self-compressed pulses at 2.1 micron from a Ho:YAG thin disk laser oscillator," in *Proc. 2017 Eur. Conf. Lasers Electro-Opt. Eur. Quantum Electron. Conf.* 2017, Paper PD_1_5.

[149] S. Vasilyev, I. Moskalev, M. Mirov, S. Mirov, and V. Gapontsev, "7 W few-cycle mid-infrared laser source at 79 MHz repetition rate," in *Proc. High-Brightness Sources Light-Driven Interact.*, 2016, Paper MT2C.4.

[150] S. Akturk, C. D'Amico, and A. Mysyrowicz, "Measuring ultrashort pulses in the single-cycle regime using frequency-resolved optical gating," *J. Opt. Soc. Amer. B*, vol. 25, pp. A63–A69, 2008.

[151] N. Leindecker, A. Marandi, R. L. Byer, and K. L. Vodopyanov, "Broadband degenerate OPO for mid-infrared frequency comb generation," *Opt. Express*, vol. 19, pp. 6296–6302, 2011.

[152] V. Smolski *et al.*, "Sub-watt femtosecond laser source with the spectrum spanning 3–8 μm," in *Proc. Laser Congr. 2017 (ASSL, LAC)*, 2017, Paper AM4A.6.

[153] K. Lee *et al.*, "Midinfrared frequency comb from self-stable degenerate GaAs optical parametric oscillator," *Opt. Express*, vol. 23, pp. 26596–26603, 2015.

[154] B. V. Dutt, O. K. Kim, and W. G. Spitzer, "Free-carrier absorption of n-type ZnSe : Al," *J. Appl. Phys.*, vol. 48, 1977, Art. no. 2110.
[155] D. Nodop, C. Jauregui, D. Schimpf, J. Limpert, and A. Tünnermann, "Efficient high-power generation of visible and mid-infrared light by degenerate four-wave-mixing in a large-mode-area photonic-crystal fiber," *Opt. Lett.*, vol. 34, pp. 3499–3501, 2009.
[156] D. V. Martyshkin *et al.*, "High average power (35 W) pulsed Fe:ZnSe laser tunable over 3.8–4.2 μm," in *Proc. Conf. Lasers Electro-Opt.*, 2015, Paper SF1F.2.

Sergey B. Mirov received the M.S. (Hons.) degree in electronic engineering from the Moscow Power Engineering Institute—Technical University, Moscow, Russia, in 1978, and the Ph.D. degree in physics from the P. N. Lebedev Physics Institute, Soviet Union Academy of Sciences, Moscow, Russia in 1983. He was a Staff Research Physicist with P. N. Lebedev Physics Institute, and a Principal Research Scientist and a Group Leader with the General Physics Institute of the Russian Academy of Sciences. Since 1993, he has been a Faculty Member with the Department of Physics, University of Alabama at Birmingham (UAB), Birmingham, AL, USA. He is currently a University Professor of Physics with the UAB, the Director of the Center for Optical Sensors and Spectroscopies, and an IPG Photonics Corporation consultant. He has authored or coauthored more than 400 scientific publications in the field of quantum electronics, 1 book, several book chapters, and holds 24 patents. His main research interests include middle-infrared laser materials, solid-state lasers, laser spectroscopy, and quantum electronics. He was the recipient of the USSR National Prize for Young Scientists in 1982. In 2004, the Institute of Electrical Engineers in the United Kingdom has named him and his team recipients of the Snell Premium Award for the input in optoelectronics and development of Cr^{2+}:ZnS mid-IR external cavity and microchip lasers. He is a Fellow of the Optical Society of America and the National Academy of Inventors, member of the IEEE Photonics Society, American Physics Society, and SPIE.

Igor S. Moskalev received the Bachelor's degree in physics from Novosibirsk State University, Novosibirsk, Russia, in 1996. He also received the M.S. and Ph.D. degrees in physics from the University of Alabama at Birmingham (UAB), Birmingham, AL, USA, in 2002 and 2004, respectively, for his work on development of ultrabroadband, multiwavelength, tunable semiconductor and Cr^{2+}:ZnSe solid-state lasers. From 1996 to 1998, he was a Research Assistant with the Institute of Laser Physics, Novosibirsk, Russia, where he was involved in development of a highly stable, single frequency, diode pumped Nd:YAG laser with intracavity frequency doubling. From 1998 to 1999, he was a Research Assistant with the Hong Kong University of Science and Technology, where he studied algal motility using a modified laser PIV system. He joined the Department of Physics, UAB, in 2000.He is currently a Senior Scientist with IPG Photonics, Southeast Technology Center, Birmingham, AL, USA, and is involved in development of novel laser systems based on semiconductor materials with transition metals impurities. With colleagues, he received the "Snell Premium" of the Institute of Electrical Engineers of the United Kingdom in 2004 for development of Cr^{2+}:ZnS mid-IR external cavity and microchip lasers.

Sergey Vasilyev received the M.S. degree in physics from the Moscow State University, Moscow, Russia, in 1995, and the Ph.D. degree in physics from the General Physics Institute, Moscow, Russia, in 1998.

From 1998 to 2002, he was a Research Associate with the Atomic Spectroscopy Laboratory, General Physics Institute. From 2002 to 2006, he was a Senior Research Associate with the Laser Materials and Technology Research Center, Moscow, Russia. From 2002 to 2011, he was a Research Fellow with the Institute for Experimental Physics, Düsseldorf, Germany. Since 2011, he has been a Laser Scientist with the IPG Photonics, Southeast Technology Center, Birmingham, AL, USA. He is the author of more than 40 articles. His research interests include nonlinear optics, quantum optics, laser spectroscopy, and laser applications.

Viktor Smolski received the Bachelor of Science degree in electrical engineering from the University of Central Florida, Orlando, FL, USA, in 2006. In 2012, he received the Ph.D. degree in electrical engineering from the University of North Carolina at Charlotte, Charlotte, NC, USA, in 2012, for his research on grating coupled surface emitting lasers. In 2013, he joined, as a Postdoctoral Associate, CREOL, University of Central Florida, where he worked on the generation of optical frequency combs in middle infrared based on optical parametric oscillators. Since 2015, he has been a Laser Scientist at IPG Photonics, Southeast Technology Center, Birmingham, AL, USA. His research interests include nonlinear optics, ultrafast lasers, optical frequency combs, laser spectroscopy, sensing, and laser development and applications.

Vladimir V. Fedorov received the M.S. degree in physical and quantum electronics from the Moscow Institute of Physics and Technology, Dolgoprudny, Russia, in 1985. He received the Ph.D. degree in physics from the Russian Academy of Sciences, Moskva, Russia, for his work on color center lasers and laser spectroscopy of the rare-earth aggregate centers in the fluoride crystals. He joined General Physics Institute, Russian Academy of Sciences, as a Research Fellow, in 1987. Since 2000, he has been with the Department of Physics, University of Alabama at Birmingham, Birmingham, AL, USA. He is currently a Research Associate Professor, and a Senior Scientist Consultant of IPG Photonics Corporation, Oxford, MA, USA. His research interests include coherent and laser spectroscopy of doped solids, nonlinear optics, color center physics, and solid-state lasers. During recent years, his research has been focused on physics of laser media based on semiconductor materials with transition metals impurities. He is a member of the Optical Society of America and the International Society for Optical Engineering. He with his colleagues received "Snell Premium" of the Institute of Electrical Engineers of the United Kingdom in 2004.

Dmitry Martyshkin received the B.S. degree in physics from Novosibirsk State University, Novosibirsk, Russia, in 1996, and the M.S. and Ph.D. degree in physics from the University of Alabama at Birmingham, Birmingham, AL, USA, in 2000 and 2004, respectively. From 2003 to 2006, he was a Scientist with Altair Center LLC, USA. From 2006 to 2010, he was a Research Associate with the University of Alabama at Birmingham. Since 2010, he has been a Research Assistant Professor with the University of Alabama at Birmingham and a consultant of IPG Photonics Corporation. He is the author of more than 40 articles. His research interests include laser spectroscopy, laser biomedical applications, and novel transitional metal-doped ternary and quaternary II–IV materials for laser applications.

Jeremy Peppers received the Bachelor of Science degree in physics from the University of West Georgia, Carrollton, GA, USA, in 2009, and the M.S. and Ph.D. degrees in physics from the University of Alabama at Birmingham (UAB), Birmingham, AL, USA, in 2014 and 2016, respectively, for his research on TM:II-VI mid-IR lasers and materials. Since 2017, he has been a Laser Scientist with IPG Photonics, Southeast Technology Center, Birmingham, AL, USA. His research interests include laser spectroscopy, laser development, and laser applications.

Mike Mirov received the Bachelor of Science degree in electrical engineering and the Master of Science degree in engineering from the University of Alabama at Birmingham, Birmingham, AL, USA, in 2006 and 2014, respectively. He was an Engineer with the Center for Biophysical Sciences and Engineering, University of Alabama at Birmingham, Birmingham, AL, USA, from 2006 to 2010. Since then, he has been with Southeast Technology Center, Birmingham, AL, USA, where he is currently the General Manager. His research interests include laser materials, laser system engineering, and mid-IR laser applications.

Alex Dergachev received the Graduate (Hons.) degree from the Department of Physics, Moscow State University, Moscow, Russia, in 1987, and the Ph.D. degree in laser physics from the General Physics Institute, Moscow, Russia, in 1991, where he started his career. From 1994 to 1997, he was a Research Assistant Professor with the University of Alabama at Birmingham. In 1997, he joined Q-Peak, Inc., Bedford, MA, USA, where he worked for 17 years. Since 2014, he has been with IPG Photonics Corporation, Marlborough, MA, USA, where he is the Head of a Laser Development Team. He is the author of numerous publications and patents. His major research interests include solid-state lasers and nonlinear optics.

Valentin Gapontsev received the Ph.D. degree in physics from the Moscow Institute of Physics and Technology, Dolgoprudny, Russia. He has been the Founder, Chairman, and Chief Executive Officer of IPG Photonics Corporation, Oxford, MA, USA, since 1990. He was a Senior Scientist in laser material physics and the Head of the laboratory at the Soviet Academy of Science's Institute of Radio Engineering and Electronics, Moscow. He has more than 30 years of academic research experience in the fields of solid-state laser materials, laser spectroscopy, and nonradiative energy transfer between rare-earth ions. He is the author of many scientific publications and several international patents. In 2006, he was the recipient of the Ernst & Young Entrepreneur of the Year Award for Industrial Products and Services in New England, and in 2009, the Arthur L. Schawlow Award by the Laser Institute of America, the Russian Federation National Award in Science and Technology in 2011. In 2011, he became a Fellow of the Optical Society of America.